ROOM TEMPERATURE ELECTROCATALYTIC CONVERSION OF METHANE TO METHANOL

BY

MUHAMMAD MUSTAPHA ADAM

A Thesis Presented to the

COLLEGE OF GRADUATE AND INTERDISCIPLINARY STUDIES

KING FAHD UNIVERSITY OF PETROLEUM & MINERALS

DHAHRAN, SAUDI ARABIA

In Partial Fulfillment of the
Requirements for the Degree of

MASTER OF SCIENCE

In

CHEMISTRY

DECEMBER 2024

KING FAHD UNIVERSITY OF PETROLEUM & MINERALS

DHAHRAN- 31261, SAUDI ARABIA

DEANSHIP OF GRADUATE STUDIES

This thesis, written by **MUHAMMAD MUSTAPHA ADAM** under the direction of his thesis advisor and approved by his thesis committee, has been presented and accepted by the Dean of Graduate Studies, in partial fulfillment of the requirements for the degree of

MASTER OF SCIENCE IN CHEMISTRY.

Prof. Basheer Chanbasha
(Advisor)

Dr. Jameel Al-Thagfi
Department Chairman

25/12/2024

Dr. Abdulrahman Al-Betar
(Member)

Dr. Suliman S. Al-Homidan
Dean of graduate studies

Dr. Sulayman Oladepo
(Member)

Date

Dedicated to Taawun Support Community Foundation

ACKNOWLEDGEMENTS

First and foremost, I give all praise and thanks to Allah, the Creator, who has granted me strength, guidance, and the wisdom to complete this work. Without His mercy, nothing would be possible. May Allah's peace and blessings be upon our noble Prophet Muhammad (PBUH), whose teachings have continually inspired me to pursue knowledge and strive for excellence, as admonished in his many traditions.

I am sincerely grateful to the Kingdom of Saudi Arabia for allowing me to pursue my academic journey. My heartfelt thanks go to KFUPM, and the Department of Chemistry for creating an environment that fosters academic growth and excellence. I deeply appreciate the resources and opportunities the university and department provided, which have played a pivotal role in my success. A special thank you to the Chairman of the Department of Chemistry, Dr. Jameel Al-Thagfi for his leadership, guidance, and inspiration throughout my academic journey.

I am deeply grateful to my advisor, Prof. Basheer Chanbasha, whose expertise, support, encouragement and mentorship have been invaluable in guiding me through my research. . I would also like to extend my thanks to the members of my committee, Dr. Abdulrahman Al-Betar and Dr. Sulayman Oladepo, for their constructive feedback and suggestions that have significantly improved my work. Special appreciation to Dr. Khalid, Dr. Tawfik and Dr. Saheed for their support.

I would like to recognize the technical staff who were instrumental in completing my experiments. Special thanks to Dr. Rajan for ensuring the timely supply of gases and chemicals, Mr. Mansur for his invaluable support in NMR analysis, and Mr. Malak, Dr.

Abdulnasar, Mr. Al-Sebaa, and Mr. Alsubaie for their contributions. I also wish to express my heartfelt gratitude to all my lab mates notably, Mr Abdullah, Juldeh and Lara. Your collaboration, advice, and encouragement have made my research journey smoother and more enriching. Working alongside you has been a privilege and a source of inspiration.

I would like to express my heartfelt gratitude to Dr. Muhammad Alhaji, Dr. Mustapha Umar, Dr. Zakariyya and Dr. Yahya Gambo for their invaluable guidance at KFUPM. I am also deeply thankful to my friends, particularly Usman Ibrahim and Hassan Umar, for their unwavering companionship. Special thanks to Ahmad Bukar, Ahmad Rufai, Faisal Lawan, Jamilu Nura, Umar Jafar, Momodou Jallow, and the entire Nigerian community at KFUPM for their steadfast support, which has been a tremendous source of strength during this challenging period. Special note also to my lifelong friends; Isa, Nazifi, Saleem and Auwal.

Finally, I reserve my deepest appreciation for my family. My father, Mal Adamu Muhammad Umar, and my mother, Fatima Yahaya, have been my lifelong role models, guiding me with their wisdom and love. I am equally grateful to my three stepmothers and my siblings: Sajida, Muhsin, Nana and her son Jafar, Nusaiba, Alamin, Abdulbasit, Hamza, Khadija, Fatima, Abdallah, Amina, Iisha, Maryam, and Musa. Your unconditional love and unwavering belief in me have been my greatest source of motivation. A special mention goes to Amina Muhammad Bello, my beloved, whose constant encouragement and faith in me have been a source of inspiration throughout this journey.

To all who have supported me, in ways big and small, I offer my sincere thanks. This achievement is as much yours as it is mine.

TABLE OF CONTENTS

LIST OF TABLES

LIST OF FIGURES

LIST OF ABBREVIATIONS

AMCSD: American Mineralogist Crystal Structure Database

EDX: Energy Dispersive X-ray Spectroscopy

GC: Gas Chromatography

GF: Graphite Felt

NMR: Nuclear Magnetic Resonance

PDMS: Polydimethylsiloxane

PPB: Parts Per Billion

PPM: Parts Per Million

RT: Room Temperature

TG: Teragram

ABSTRACT

Full Name : Muhammad Mustapha Adam

Thesis Title : Room temperature electrocatalytic methane conversion to methanol

Major Field : Chemistry

Date of Degree : December 2024

Methane conversion to value-added chemicals, such as methanol, offers a promising strategy for both mitigating greenhouse gas emissions and enabling sustainable chemical production. Traditional industrial methods, which rely on energy-intensive processes at high temperatures and pressures, contrast with direct methane conversion, especially using electrocatalysis as a more energy-efficient alternative under milder conditions. In this study, Fe_2O_3 catalysts were synthesized via a hydrothermal method and deposited onto graphite felt electrodes, which were used in a flow cell reactor for methane conversion at room temperature. The products were detected and analyzed using gas Chromatography and Nuclear Magnetic Resonance. Reaction optimization, including the applied voltage and electrolyte composition, improved the system performance. We observed a methane conversion efficiency of 37%, with 100% methanol selectivity and a methanol yield of 873 μmol/g/hr when using water as the oxidant. The addition of 3% potassium chloride further increased the yield to 1,248 μmol/g/hr, maintaining 100% methanol selectivity. These findings highlight a low temperature, electrocatalytic pathway for methane conversion, offering a sustainable approach to chemical synthesis and broad potential for greenhouse gas utilization.

ملخص الرسالة

الاسم الكامل: محمد مصطفى أدم

عنوان الرسالة: تحويل الميثان إلى ميثانول بالتحفيز الكهربائي في درجة حرارة الغرفة

التخصص: الكيمياء

تاريخ الدرجة العلمية: ديسمبر 2024

تحويل الميثان إلى مواد كيميائية ذات قيمة مضافة، مثل الميثانول، يقدم استراتيجية واعدة لكل من التخفيف من انبعاثات غازات الدفيئة وتمكين الإنتاج الكيميائي المستدام. تتناقض الطرق الصناعية التقليدية، التي تعتمد على عمليات كثيفة الطاقة عند درجات حرارة وضغوط عالية، مع التحويل المباشر للميثان، خاصة باستخدام التحفيز الكهربائي كبديل أكثر كفاءة في استخدام الطاقة تحت ظروف أكثر اعتدالًا. في هذه الدراسة، تم تخليق محفزات F_e2O_3 عبر طريقة الهيدروحرارية وتم إيداعها على أقطاب مصنوعة من ألياف الجرافيت، والتي استخدمت في مفاعل خلية تدفق لتحويل الميثان عند درجة حرارة الغرفة. تم الكشف عن المنتجات وقياسها باستخدام الكروماتوغرافيا الغازية والرنين المغناطيسي النووي. أدى تحسين التفاعل، بما في ذلك الجهد المطبق وتركيب الإلكتروليت، إلى تحسين أداء النظام. لوحظت كفاءة تحويل الميثان بنسبة37% ، مع انتقائية 100% للميثانول وعائد ميثانول قدره 873 ميكرومول/غرام/ساعة عند استخدام الماء كإلكتروليت. زادت إضافة 3% من كلوريد البوتاسيوم العائد إلى 1,248 ميكرومول/غرام/ساعة، مع الحفاظ على انتقائية 100% للميثانول. تسلط هذه النتائج الضوء على مسار تحفيزي كهربائي عند درجات حرارة منخفضة لتحويل الميثان، مما يقدم نهجًا مستدامًا لتخليق المواد الكيميائية وإمكانية واسعة لاستخدام غازات الدفيئة.

CHAPTER 1

INTRODUCTION

1.1 Methane emissions

Methane is the most abundant natural resource and is a potent greenhouse gas with significant implications for climate change and energy sustainability [1]. Methane ranks as the second most significant factor in global warming, following carbon dioxide. Over a 20-year period, methane's effect on global warming is roughly 80 times stronger than CO_2 [2] and it has been about 30 times more impactful over the past century [3]. Methane is chemically reactive in the Earth's atmosphere, where its oxidation results in the formation of greenhouse gases such as tropospheric ozone, carbon dioxide, and stratospheric water vapor. Additionally, tropospheric ozone significantly contributes to air pollution [4]. Methane emissions account for about 10% of global greenhouse gas emissions, with a notable fraction resulting from anthropogenic activities such as agriculture, waste management, and fossil fuel extraction [5]. While methane's emissions worsen global warming, its high energy content and availability make it a valuable feedstock for producing fuels and chemicals [6]. Utilizing methane effectively represents an opportunity to mitigate environmental impacts while creating sustainable energy and chemical supply chains [7]. Approximately 1% of these emissions directly emanate from the petroleum industry through processes such as gas flaring [8]. The greenhouse gas composition and methane sources in the US for the period 1990–2022 based on the EPA's 2023 report are depicted in Figure 1.1 below. The data shows that carbon dioxide is the dominant greenhouse gas, accounting for 79.4% of total emissions, followed by methane at 11.5%, nitrous oxide at 6.2%, and fluorinated gases at 3.0 %. Methane emissions are further broken down by source, with enteric fermentation from livestock as the largest contributor (25 %), followed by landfills (15 %), natural gas and petroleum systems (26%), and smaller contributions from manure management, coal mining, and flooded land.

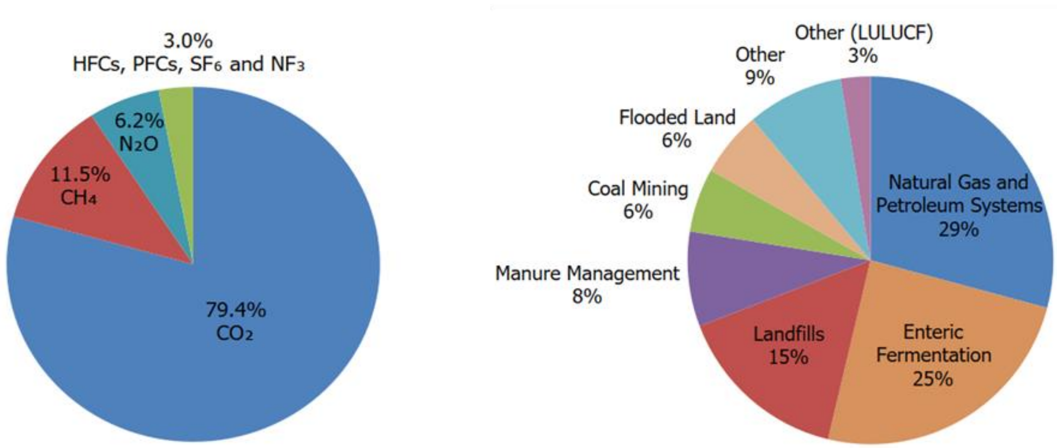

Figure 0.1 Greenhouse composition and methane emission sources [9]

1.2 Methane conversion

Converting methane into value-added products has become an important area of research and industrial development due to its potential to provide sustainable alternatives to fossil fuel-based energy and chemical production [10]. It holds great potential for providing a sustainable supply of energy fuels and chemicals without reliance on crude oil in the future [11]. It provides a dual advantage in addressing the issue of gas flaring by transforming waste into valuable resources while also promoting environmentally sustainable practices [12]. Methane oxidation improves air quality by lowering surface ozone concentrations. For every Tg of methane oxidized per year, global surface ozone decreases by approximately 0.012 ± 0.002 ppb, preventing an estimated 600 premature deaths annually

[13]. However, cleaving the first C-H bond in methane is challenging due to its high bond dissociation energy (439.3 kJ/mol) and high ionization potential (13.0 eV) [14].

1.2.1 Traditional method of methane conversion

Leading petrochemical industries have adopted the conversion of CH_4 to valuable chemicals [15]. The approach has utilized a dual-phase technique that converts methane into synthesis gas through steam reforming. The second step involves catalytic conversion of syngas into methanol through processes like Fischer-Tropsch or methanol synthesis [16]. Methanol is a versatile C_1 compound with a high energy density, ease of transport, and an established global market [17]. It is a precursor in the production of formaldehyde, acetic acid, and dimethyl ether. [18] These derivatives are essential for manufacturing polymers, adhesives, resins, and synthetic fibers, which are vital in industries such as construction, automotive, and textiles [19]. However, the syngas approach is a costly and energy-intensive process However, the syngas route is energy-intensive, requiring high temperatures (700–1000 °C) and pressures (up to 50 bar), resulting in significant operational costs and greenhouse gas emissions [20]. These limitations drive the need for alternative, more sustainable methane conversion methods.

1.2.2 Direct conversion

Direct conversion of methane to methanol represents a promising alternative, offering the potential for high energy efficiency under milder conditions. Unlike the energy-intensive indirect processes involving syngas as an intermediate, direct conversion overcomes high-temperature reforming and multi-step synthesis, enabling simpler and potentially more sustainable methane utilization pathways [21]. Among the emerging technologies, electrocatalytic methods have gained significant attention due to their ability to activate methane selectively without extreme temperatures or pressures, making them more compatible with renewable energy sources. However, these processes are hindered by challenges such as the inertness and strength of methane's C-H bond [22]. Even when activation occurs, methanol as a product tends to over-oxidize on most catalysts, leading to products such as CO or CO_2 [23]. This preference for deep oxidation stems from the catalytic surfaces, which often favor the formation of highly reactive oxygen species unsuitable for selective methanol production [24]. Additionally, achieving selectivity for methanol remains a major hurdle due to its higher reactivity compared to methane [25]. Another major issue is the low solubility of methane in aqueous systems, which limits the availability of the reactant at the catalyst surface results in mass transport limitations that hinder overall reaction efficiency [26].

The success of direct methane conversion hinges on several factors: 1) The development of catalysts with high activity, stability, and selectivity; [27] 2) the selection of oxidants that enable the controlled formation of active oxygen species is essential for driving selective oxidation reactions; [28] Optimization of reaction conditions, including temperature, reactant concentration, and applied potential; and [29] ensuring the process operates at current densities suitable for industrial application remains a major hurdle. Scaling up laboratory results to industrially relevant conditions require overcoming challenges related to system stability and energy efficiency [2]. Addressing these factors can pave the way for a sustainable and economically viable methane utilization pathway. Figure 1.2 below shows a comparison between the industrial indirect methane conversion via syngas and the direct conversion method.

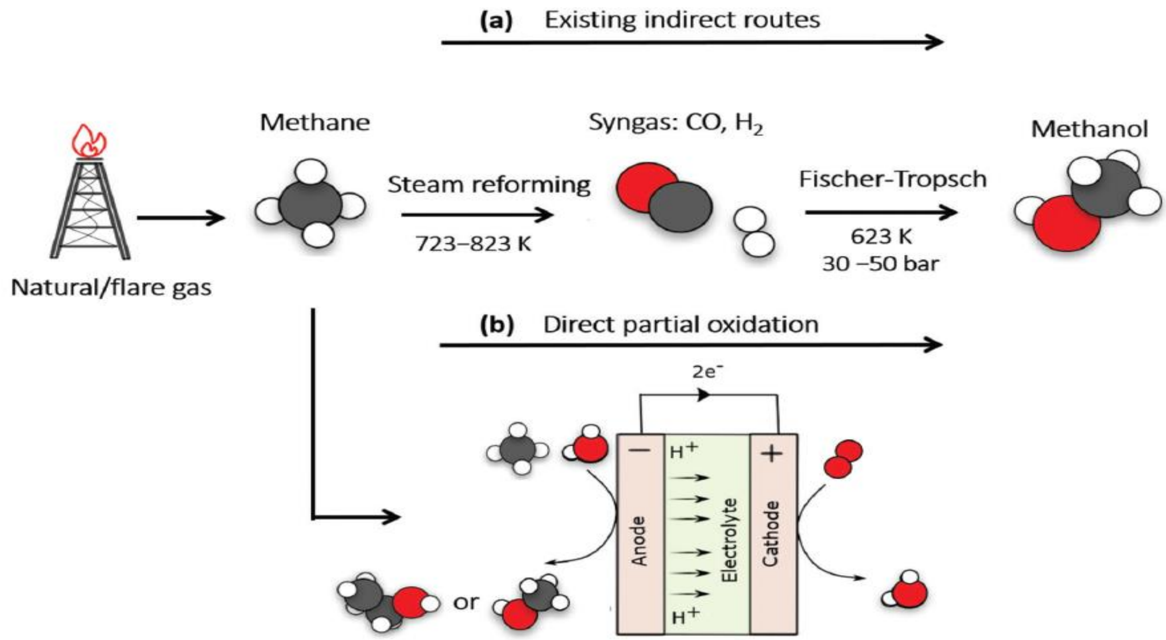

Figure 1.2 Traditional and current methods of methane conversion [29]

1.2.3 Room-Temperature Conversion

As opposed to methane conversion which operates at high temperatures, the room-temperature approach utilizes innovative techniques such as electrochemical, photocatalytic, or plasma-based activation to efficiently convert methane into value-added products like methanol or acetic acid [30]. This drastically reduces energy consumption, resulting in lower carbon footprints and making these methods ideal for addressing global sustainability goals. Additionally, low-temperature conditions inherently favor higher liquid products selectivity by suppressing secondary reactions that often lead to overoxidation to undesired by-products [31]. By eliminating the need for extensive heating infrastructure and aligning with green energy solutions, room-temperature methane conversion represents a transformative advancement in sustainable chemistry [32].

This study explores the use of Fe_2O_3-based electrocatalysts for methane-to-methanol conversion in a flow cell system operating at room temperature. The flow cell system employed in this study provides a controlled environment to optimize reaction parameters and enhance product selectivity. Flow cell technology has revolutionized the approach to electrocatalytic methane conversion by enabling continuous operation, as opposed to the batch processes traditionally used. Continuous operation ensures a consistent supply of reactants—methane and oxygen—while facilitating the real-time removal of products, such as methanol, from the reaction interface. This design enhances mass transfer, promotes efficient reaction kinetics, and is scalable for industrial applications. By utilizing Fe_2O_3's catalytic properties, this research aims to address key limitations in methane conversion and contribute to the development of efficient electrocatalytic systems.

1.3 Objectives of the study

This thesis is aimed at developing an efficient direct methane conversion of methane to methanol. The primary objectives are as follows:

1. Synthesize and characterize Fe_2O_3 while enhancing its conductivity through coating on graphite felt.

2. Evaluate the catalyst's performance for electrocatalytic conversion of methane to methanol in a flow cell at room temperature and analyze the resulting products using gas chromatography and nuclear magnetic resonance.

3. Systematically investigate and optimize reaction parameters to increase methanol yield.

4. To evaluate the effect of salt water by adding Potassium Chloride and investigate the effect on methanol yield.

CHAPTER 2

LITERATURE REVIEW

This chapter reviews the latest progress in electrocatalytic systems for methane partial oxidation, with a focus on catalyst design, reaction parameters, and the role of oxidants in achieving high product selectivity and yield.

2.1 Methane partial oxidation

Recent advances in mild methane oxidation have focused on reducing the severe thermodynamic and kinetic challenges associated with activating methane's strong C–H bond. Researchers have explored various pathways, including bio-catalysis, homogeneous catalysis, low-temperature heterogeneous catalysis, photocatalysis, and electrocatalysis [3]. Heterogeneous catalysis employs the use of enzyme to selectively convert methane to methanol, however, the high cost purifying the enzymes and difficulty to scale up remains a challenge. Homogeneous catalysis suffers from catalyst recycling and recovery. Thermal catalysis is not desired because it is energy intensive. Among these, photocatalytic and electrocatalytic approaches stand out for their ability to lower the energy barrier for methane activation under mild conditions, thereby minimizing energy consumption and the risk of overoxidation to carbon dioxide [22]. Photocatalysis encounters significant obstacles, including low efficiency in solar energy conversion, high rates of recombination for photogenerated carriers, intricate catalyst engineering requirements, and the high cost of oxidants such as hydrogen peroxide. On the other hand, electrocatalytic oxidation presents a potentially advantageous alternative, as the redox process based on interfacial charge transfer can be managed with greater precision and control. [30]. Figure 2.1 presents an overview of various catalytic systems used for methane-to-methanol conversion. Meanwhile, Figure 2.2 below outlines two mechanisms: (a) Direct methane activation and (b) Indirect methane activation, which involves catalytic species capable of regenerating on the electrode surface (represented by pink arrows) or the formation of radical species through electro generation (indicated by red arrows).

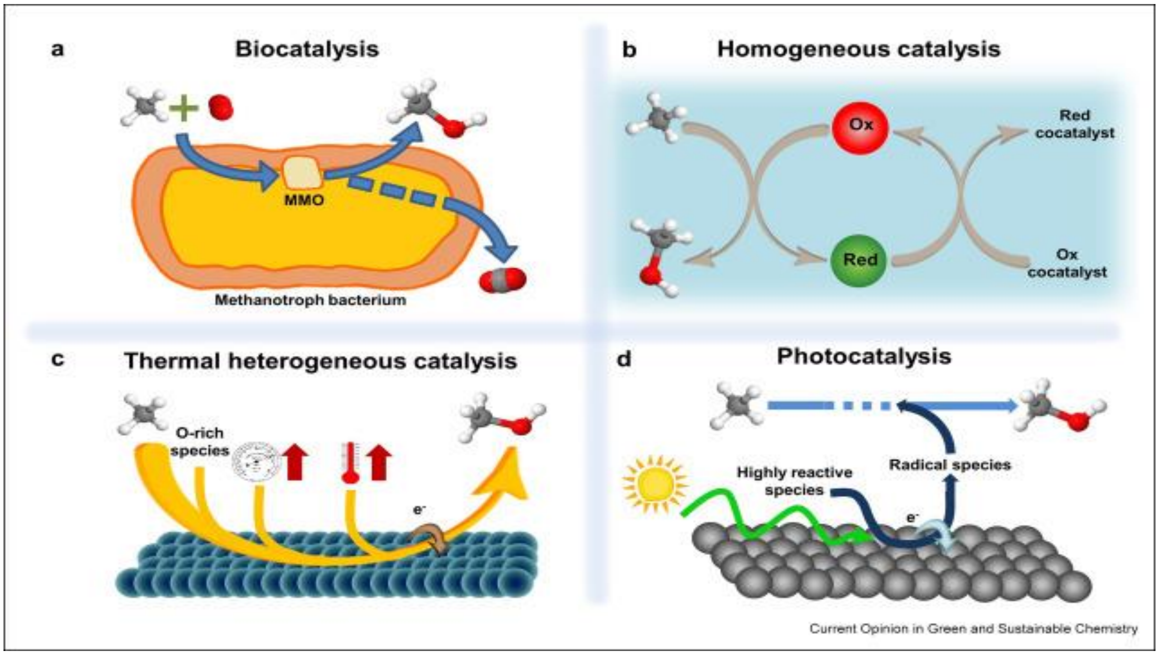

Figure 2.1 Schematics for different catalytic approaches to methane conversion [33]

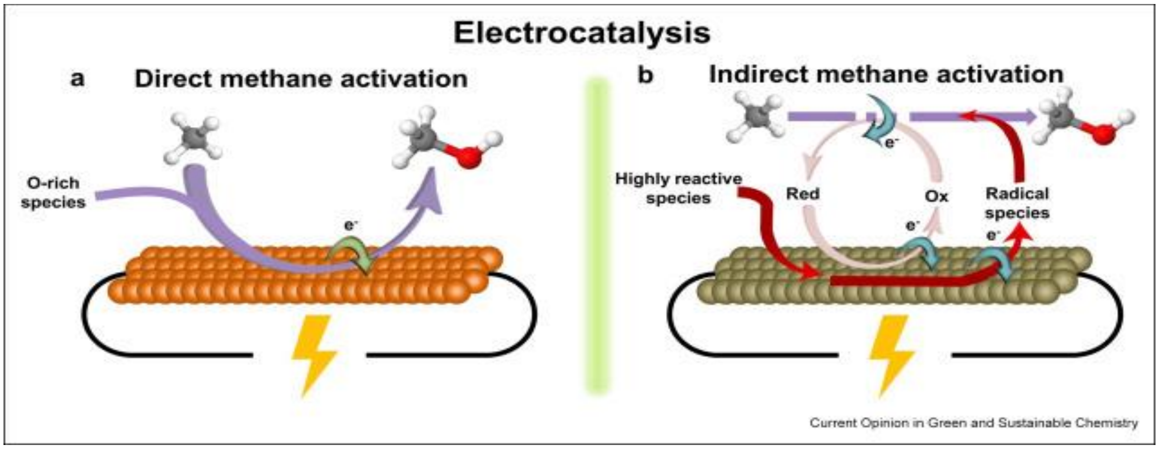

Figure 2.2 Direct and indirect electrocatalytic methane conversion methods [33]

2.2 Electrochemical cell parameters

2.2.1 Catalyst design and Performance

Catalysts are pivotal in the selective oxidation of methane, as they facilitate the activation of the C–H bond and control reaction pathways to yield desired products while suppressing undesired overoxidation. The ideal catalyst must combine high activity, selectivity, and stability under the reaction conditions [34].

2.2.1.1 Transition metal oxides

Among metal oxides, vanadium-based catalysts have shown significant promise. Lee et al. reported that V_2O_5/SnO_2 demonstrated remarkable performance, achieving a current efficiency of 61.4% and a selectivity of 88.4% for methanol production at 100°C [35]. Similarly, TiO_2/RuO_2/PTFE-based gas diffusion electrodes have been employed for methane oxidation in neutral aqueous electrolytes, leveraging the high activity of these oxides for selective oxidation [36]. These studies highlight the potential of metal oxides, particularly SnO_2 and TiO_2, which exhibit low activation energies for C–H bond activation while minimizing oxygen evolution reaction (OER) side pathways [37].

2.2.1.2 Zeolite-Supported Catalysts

The integration of metal species into zeolite frameworks has gained attention for enhancing selectivity and stability. Wu *et al.* [38] demonstrated that Fe-binuclear sites on ZSM-5 selectively converted methane to acetic acid with 100 % selectivity for oxygenates at 30 °C. Among the oxygenated products, acetic acid accounted for 66%, while methanol, formic acid and methyl hydroperoxide were also detected. This study is particularly noteworthy for achieving ultrahigh selectivity under ambient conditions, However, the amount of product generated per unit reactor volume per unit time remains low. This indicates that while the process is highly selective, the rate of acetic acid production is insufficient for industrial-scale applications.

2.2.1.3 Photocatalysts for Methane Oxidation

Photocatalysis offers an alternative strategy by utilizing light energy to activate methane under mild conditions. Han *et al.* developed a photocatalytic system that selectively produced methanol and formic acid at room temperature, with a C_1 product selectivity of nearly 99%. The oxygen content in the reaction system controlled the dual reaction pathways, enabling targeted production of methanol or formic acid. This innovative approach avoids harsh oxidants and extreme temperatures, but its scalability remains a significant limitation [39].

2.2.1.4 Iron-Based Catalysts

Iron-supported ZSM-5 catalysts have also demonstrated efficiency in methane oxidation under mild conditions. Zhu *et al.* [40] reported a system operating at 80°C that achieved 91 % selectivity toward formic acid among C_1 oxygenates, with methanol and methyl hydroperoxide as minor products.

Iron oxides have shown promise as catalysts in such systems. These materials facilitate the generation of active oxygen species, which are essential for breaking methane's C-H bonds [41]. Iron-based oxygen carriers demonstrate a minimal tendency for coke formation and possess significant resistance to agglomeration, both of which are essential for catalyst activity throughout ongoing redox cycles [42].

Iron (III) oxide (Fe_2O_3) has gained attention for its potential as an electrocatalyst in methane-to-methanol conversion. Its abundance, cost-effectiveness, and favorable redox properties make it an attractive alternative to noble metal catalysts. Fe_2O_3 operates effectively under mild conditions, offering high selectivity for methanol while suppressing undesired side reactions such as complete oxidation to CO_2 [43]. Fe_2O_3 has demonstrated its effectiveness in electrochemical methane oxidation. Al-Attas *et al*. [44] explored its role in the formation of high-valence Iron-oxo species FeO, which initiate CH_4 activation via hydrogen abstraction. This mechanism enabled the production of oxygenated chemicals, such as methanol and acetone, under ambient conditions while limiting overoxidation. Zhang *et al.* [45] explored the use of Fe_2O_3 for methane-to-formic acid conversion under mild conditions. The Fe_2O_3 phase supports a radical-driven mechanism initiated by hydroxyl radicals (·OH), which selectively oxidizes methane through intermediates like methanol and methyl hydroperoxide to formic acid while minimizing overoxidation to undesired by-products such as carbon dioxide. Zhou *et al*. [46] demonstrated that Fe_2O_3, when combined with WO_3, enhances methane oxidation through efficient charge separation and the generation of reactive radicals like chlorine. Fe_2O_3 facilitates selective activation of methane, minimizing overoxidation and enabling the production of valuable intermediates. These properties justify Fe_2O_3 as a reliable catalyst for selective and sustainable methane utilization in various oxidation processes.

2.2.2 Temperature Influence

The reaction temperature significantly influences methane oxidation pathways and product distribution. High-temperature gas-phase reactions, while kinetically favorable, often result in overoxidation of methanol to CO_2, suffer from catalyst deactivation and [47] reduction in methane solubility [48]. Conversely, low-temperature liquid-phase systems, particularly those operating below 100 °C, are advantageous for selective methane oxidation due to their ability to mitigate overoxidation and enhance catalyst stability [49].

2.2.2.1 Room-Temperature Systems

Cui *et al.* demonstrated the successful conversion of methane to methanol using single iron atoms on graphene with H_2O_2 as an oxidant. The system achieved excellent activity at room temperature, underscoring the potential of atomically dispersed catalysts for mild methane activation [50]. Similarly, Nandenha *et al* [51] employed a proton exchange membrane fuel cell to generate hydroxyl radicals for methane oxidation, achieving promising results under ambient conditions.

2.2.3 Cell configuration

The oxidation of methane has been explored in both non-aqueous and aqueous electrolyte cells and membrane electrode assembly (MEA) known as full cells, each providing unique advantages [52]. Aqueous electrolyte cells are valuable for swiftly evaluating catalytic activity as well as the working electrode's selectivity, however, they are limited in achieving the desired current densities necessary for industrial application due to inefficient mass transfer and the limited dissolution of methane in water-based electrolytes, restricting the current density to less than 20 $mAcm^{-2}$. MEAs provide improved mass transport and scalability, offering better prospects for industrial adoption [53].

One promising system for methane-to-methanol conversion is the membrane electrode assembly (MEA) architecture [54]. MEAs enable efficient transport of reactants and products to and from the catalyst layer while minimizing ohmic losses across the membrane. These assemblies are configured as either fully vapor-fed systems or with liquid electrolyte solutions supplied to one or both sides of the cell. Such configurations regulate pH and optimize the microenvironment for the reaction [55].

2.2.4 Oxidant

Oxidants are critical for initiating methane oxidation by generating active oxygen species that drive the reaction. The choice and concentration of the oxidant significantly influences reaction efficiency and product selectivity. Commonly employed oxidants include water, hydrogen peroxide and oxygen. The ideal oxidant concentration depends on the specific reaction conditions and the desired products [56].

In electrochemical partial methane oxidation, oxidants are essential for producing active oxygen species required for initiating the reaction [29]. Freakley *et al* [57] investigated the use of AuPd colloids and Cu-promoted Fe-zeolites as catalysts in systems that utilized both H_2O_2 and O_2 as oxidants in a water solvent at 60 °C. While effective, the high cost of H_2O_2 limits its feasibility for large-scale commercialization.

2.2.4.1 Water as oxidant

Water has been explored as a cost-effective and environmentally friendly oxidant in methane oxidation. Luo *et al.* [58] used a system that combined oxygen with gold single atoms on black phosphorus nanosheets. Under light irradiation at 90 °C, this system produced hydroxyl radicals for the mild oxidation of methane to methanol. Water is particularly advantageous for methane-to-methanol conversion because it enhances methanol desorption and generates active oxygen species on the catalyst surface. This promotes hydrogen abstraction from methane while maintaining room temperature conditions [29]. Additionally, it facilitates two potential mechanisms: blocking active sites for methanol dissociation or creating a new reaction pathway for the direct interaction of CH_4 or CH_3 with OH groups [59].

Thermodynamically, the Gibbs free energy difference for methane oxidation to methanol versus complete oxidation to CO_2 is 9 kJ/mol. This narrow margin underscores the feasibility of achieving selective methanol production at significant conversion levels with the aid of suitable electrocatalysts [54].

Table 2.1 summarizes some of the most important reports on the electrocatalytic methane conversion to valuable chemicals. The metric of comparing the reports is difficult because of the parameters involved in the process. Also, some of the configurations or performance were missing either because they were not applicable, or the author did not report. These trends highlight how the integration of cell components, such as catalysts, oxidants, and electrode design, influences the overall performance of methane electrooxidation. Three electrode cells, two electrode cells having exchange membrane and gas diffusion electrodes were all reported and summarized. The table also shows the use of many electrocatalysts to activate methane at room temperature and higher temperatures. A few of the reports summarized used precious metals which means the activation can be done using cheap and abundant electrocatalysts. Expensive oxidants such as H_2O_2 Oxidants were avoided in most of the reports and others such as CO_3^{2-} were used at room temperature to produce oxygenates without overoxidation products but often lack selectivity to a single product. Water as a fascinating oxidant was used at elevated temperatures. reported electrocatalytic conversions at room temperature or near room temperature were not selective to one liquid product. It is worth noting that there exists a gap for achieving high methanol selectivity using an inexpensive and environmentally friendly oxidant at room temperature.

Table 2.1 The influence of different components in electrochemical systems on methane conversion and product selectivity

Cell Design	Catalyst	Oxidant	T (°C)	Potential	Products	Selectivity (%)	Ref.
GDE	CuO_X – PdAu/C	O_2	300	-	CH_3OH	100	[60]
GDE	V_2O_5/SnO_2; PTFE	H_2O	100	0.9	CH_3OH, CO_2	88.4	[61]
Two electrodes (PEM)	Pt/C	H_2O_2	85	0.5	CH_3OH	-	[62]
Two electrodes cell (CEM)	NiO-ZrO_2	CO_3^{2-}	40	2	CH_3OH, HCHO, CO, HCOOH, CH_3CH_2OH, CH_3COOH, CH_3COCH_3	-	[63]
Three electrodes cell	Co_3O_4-ZrO_2	CO_3^{2-}	RT	2.0	$CH_3CH_2CH_2OH$ $(CH_3)_2CHOH$, CH_3CHO, CH_3OH, CH_3CH_2OH	60	[64]
Three electrodes cell	CuO/CeO_2	CO_3^{2-}	RT		CH_3OH, C_2H_5OH, CH_3COCH_3	79	[65]
Three electrodes cell	NiO/ZnO	CO_3^{2-}	RT	1.5	C_2H_5OH, CH_3OH, CH_3COCH_3	81	[66]
Three electrodes cell	Zr-Fe_2O_3	CO_3^{2-}	RT	1.6	CH_3OH, CH_3CH_2OH	91	[67]
Three electrodes cell	Pd/graphite	H_2O	RT	0.64	CH_3OH, CH_3CH_2OH	-	[68]
Two Electrodes cells (HOM)	Pd/C	OH^-	80	0.3	CH_3OH	-	[69]

CEM, Carbonate Exchange Membrane; PEM, Proton Exchange Membrane; HOM, hydroxide Exchange Membrane.

2.3 Catalyst-free methane oxidation

Richard Zare recently reported interesting exceptions found in several studies [34], [70]. When the size of water droplets is reduced and an electric charge is applied, the water behaves differently. This change leads to the creation of H^+ and OH^- ions and radicals, occurring both with and without the electric charge. They recently developed droplet assisted way to produce methanol from methane gas at ambient temperature without any photocatalyst or electrocatalyst.

Water Microdroplets-Initiated Methane Oxidation by Richard Zare [71] introduces an innovative approach for methane conversion without the need for catalysts, using water microdroplets to initiate the reaction. Methane oxidation is achieved by reactive oxygen species (ROS) generated at the interface of water microdroplets and methane. The process relies on the formation of radicals, such as hydroxyl (OH•), which enable partial oxidation of methane to methanol under mild conditions. Although the conversion efficiency remains modest compared to other catalytic systems, this method presents a more environmentally friendly and simple approach to methane oxidation.

Li et al [72] introduced a novel approach for methane activation using water microbubbles under ambient conditions, eliminating the need for a catalyst or external oxidizing agents. The microbubbles create a high gas-liquid interfacial area, which facilitates the generation of hydroxyl (OH·) and hydrogen (H·) radicals. These radicals are key to methane activation, enabling partial oxidation. The primary products obtained are ethane and formic acid, with production rates of 23.5 ppm/h and 2.3 nM/h, respectively. The process achieves a methane activation rate of 6.7 % per hour, which is significantly enhanced by optimizing bubble size (50 μm), water temperature (15°C), and gas-liquid interaction time (150 s). A continuous operation over 8 hours yielded a methane conversion rate of 171.5 ppm/h. The study demonstrates high stability and scalability, supported by detailed analyses using gas chromatography and electron spin resonance spectroscopy.

CHAPTER 3

METHODOLOGY

3.1 Materials

Porous graphite felt with dimension 100 x 100 x 10 mm was purchased from Jiangsu Sutong Carbon fiber Co. Ltd China. $FeCl_3 \cdot 6H_2O$ and Na_2CO_3 were sourced from Sigma-Aldrich, while KCl was obtained from BDH Laboratory Supplies. Ethanol was purchased from Honeywell, methanol from BDH Chemicals Ltd (Poole, England), and isopropanol from ITW Reagents. Nafion™ PFSA 5 % Dispersion - D521 from Ion Power was used for catalyst preparation. Our gas supplies included methane, hydrogen, zero air, and Helium, all provided by Abdullah Hashim Industrial Gases & Equipment Co. Ltd. All solutions were prepared using distilled water.

3.2 Preparation of Fe_2O_3

Fe_2O_3 was synthesized using a hydrothermal synthesis method. Initially, 1.37 g of $FeCl_3 \cdot 6H_2O$ was dissolved in 50 mL of deionized water. A 2 mol/L Na_2CO_3 solution was then added dropwise until the pH reached 9 which was essential for precipitating the Fe_2O_3. The mixture was processed at 200 °C for 12 hours, followed by centrifugation by washing with water and ethanol followed by oven drying to obtain Fe_2O_3 samples [73]. The synthesis is illustrated in Figure 3.1 below. The synthesis involves generation of FeOOH which is dehydrated to produce Fe_2O_3 as shown in equations 1 and 2.

$$FeCl_3 + OH^- \rightarrow FeOOH \tag{1}$$

$$FeOOH \rightarrow Fe_2O_3 \tag{2}$$

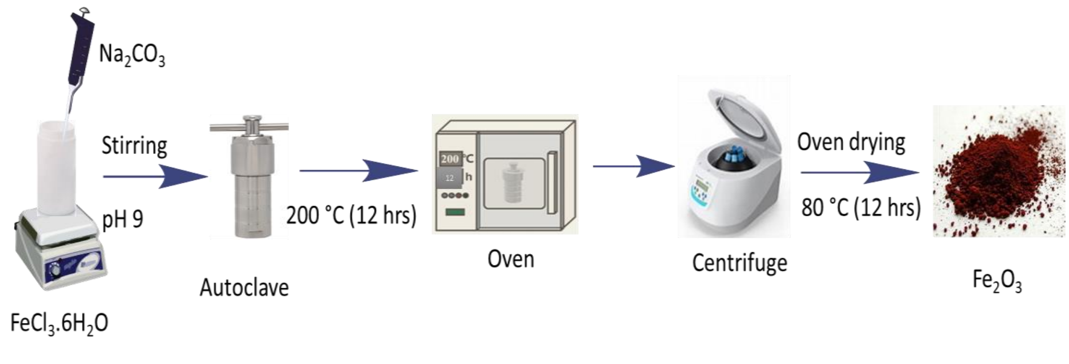

Figure 3.1 Hydrothermal synthesis of Fe_2O_3

3.3 Preparation of catalyst electrode

The catalyst electrode preparation followed a modified method [74]. A homogeneous ink was produced by dispersing 5.0 mg of catalyst and 40.0 µL of Nafion solution (1.66 wt%) in a mixture of 600 µL isopropanol and 360 µL water through ultrasonication for 60 minutes. This dispersion was then sprayed as microdroplets onto a graphite felt electrode substrate (3.0×3.0 cm^2) for even coating. The coated electrode was dried in an oven at 85 °C for 60 minutes and subsequently allowed to cool to ambient temperature, resulting in a catalyst loading of 0.56 mg cm^{-2}. Figure 3.2 shows the preparation of the catalyst electrode. The catalyst electrode was used as the anode in the electrocatalytic reactions.

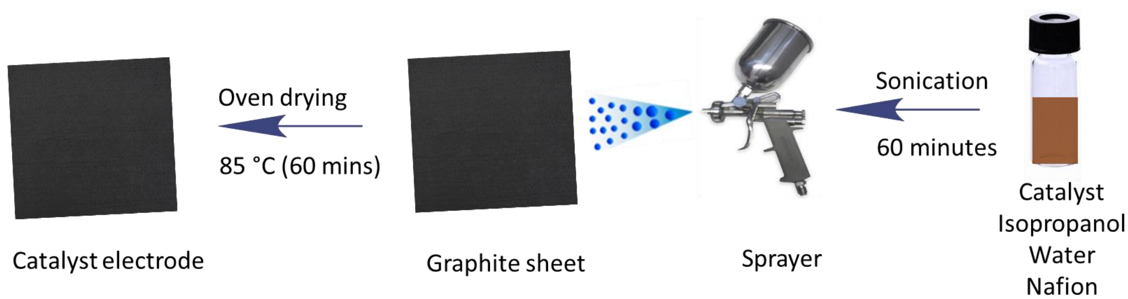

Figure 3.2 Preparation of the catalyst electrode (GF-Fe_2O_3)

3.4 Catalyst Characterization

3.4.1 X-ray Diffraction

X-ray diffraction (XRD) analysis was performed to characterize the crystallinity and phase composition of the synthesized catalysts. A Rigaku Ultima IV XRD with Cu Kα radiation was utilized, scanning a 2θ range from 20° to 80° at a rate of 2° per minute.

3.4.2 Scanning Electron Microscopy (SEM)

The sample's surface morphology was examined with a Thermo Scientific Quattro S scanning electron microscope (SEM). High-resolution images were produced by capturing secondary electrons from a focused electron beam. The SEM operated at an accelerating voltage of 10 kV, offering a magnification range up to 200,000x, with a working distance of 10.3 mm, a spot size of 3.5, and a pressure between 1.006 and 3 Pa.

3.4.3 Fourier Transform Infrared Spectroscopy (FTIR)

FTIR was employed to obtain the infrared absorption spectrum of the sample. The sample was exposed to infrared light, and the transmitted light was recorded to produce a spectrum. The analysis was conducted using a Thermo Scientific Nicolet iS10 FT-IR Spectrometer and Nicolet iZ10 Module from 600 to 4000 cm^{-1}.

3.5 Electrochemical setup

The electrochemical methane-to-methanol conversion experiment was conducted in a flow cell divided into two compartments: the anode and the cathode chambers. Each chamber was equipped with gas inlets and outlets and separated by a proton-exchange membrane to prevent mixing of the electrolytes while enabling proton (H^+) transfer. The anode chamber housed a Fe_2O_3-coated graphite felt electrode mounted on stainless steel, while the cathode consisted of a stainless-steel electrode. Methane gas was introduced into the anolyte loop, with and without oxygen, to assess the effect of gas composition on product formation.

A peristaltic pump circulated the anode and cathode electrolyte solutions through the reactor, ensuring a continuous and steady flow. The electrolyte flow was divided into two pathways: the anodic path (blue) and the cathodic path (green). The pump maintained a constant supply of electrolyte, with the anodic path carrying the electrolyte across the anode to facilitate methane oxidation and product formation. Simultaneously, the cathodic path delivered the electrolyte to the cathode where reduction reactions occurred. Both electrolytes exited their respective compartments and were circulated again until the desired time for sample collection. A check valve was installed in the gas line to prevent backflow and contamination of the gas supply, ensuring a steady flow of methane and oxygen where applicable.

During the experiment, a direct current (DC) power supply applied a voltage across the electrodes to drive the electrochemical reactions. Optimization of the reaction conditions was carried out by systematically varying one parameter at a time while keeping the others constant. The optimized parameters included applied voltage, electrolyte flow rate, gas pressure, electrolyte volume, and reaction time. Once the optimal reaction conditions were determined, the experiment was conducted under these optimized parameters and analyzed further. The schematic representation of the experimental setup is shown in Figure 3.3, with an enlarged view of the flow cell provided in Figure 3.4. This setup enabled efficient and continuous electrolyte circulation, precise control over reaction conditions, and separate collection of anodic and cathodic products.

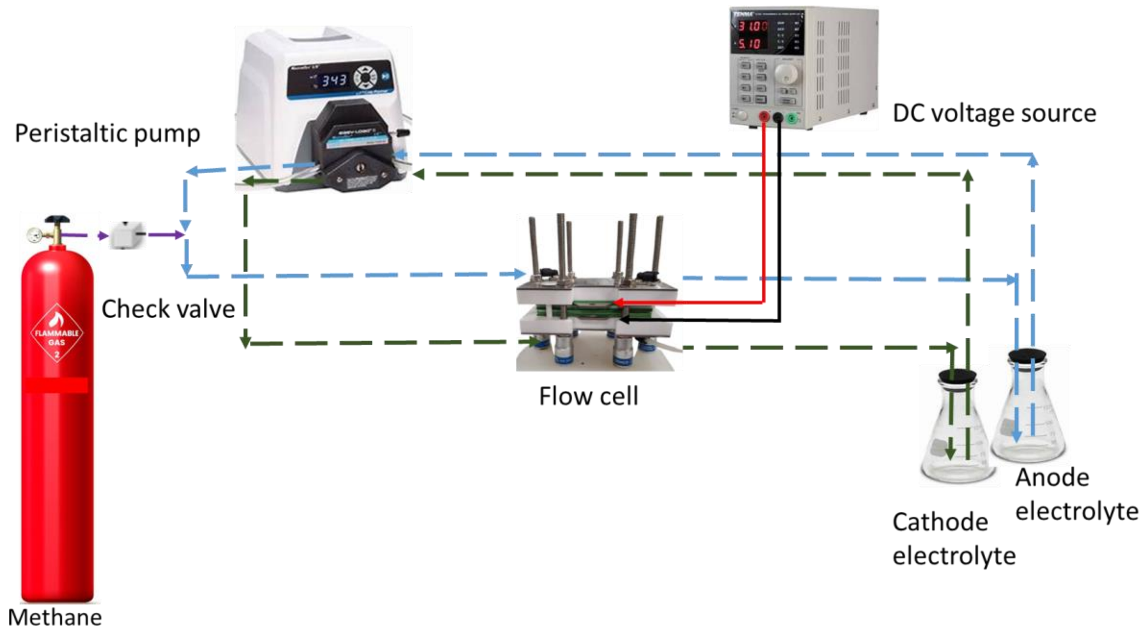

Fig. 10: Flow cell reaction setup

Figure 0.3 Electrochemical set up

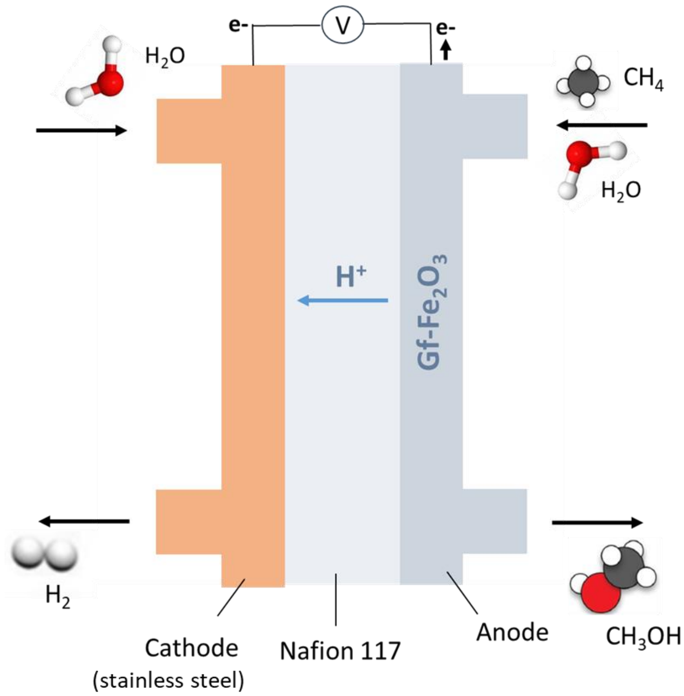

Figure 3.4 Flow Cell configuration

3.6 Solid Phase Micro Extraction (SPME)

10 mL of the reaction products were transferred to a glass vial and placed on a magnetic stirrer to ensure homogeneous mixing. SPME fiber coated with a PDMS selective adsorbent was dipped directly into the solution while stirring continuously for 20 minutes, allowing volatile analytes to adsorb onto the fiber. After the extraction period, the SPME fiber was introduced into the gas chromatograph (GC) injection port, where thermal desorption released the adsorbed compounds for analysis.

3.7 Gas chromatography Analysis

Methanol in sprayed water samples was quantified using a gas chromatograph (GC) with a flame ionization detector (FID). The GC-FID conditions included a Supelco wax column with a length of 60 meters and an internal diameter ranging from 0.25 to 0.32 mm. Helium served as the carrier gas with a flow rate of 1 mL/min. The temperature program started at 70 °C, maintained for 2 minutes, and then increased at a rate of 8°C per minute until it reached 250 °C. The FID temperature was set at 250°C for the analysis.

3.8 Nuclear Magnetic Resonance Analysis

The product samples were analyzed using nuclear magnetic resonance (NMR) spectroscopy on a JEOL ECZLR 600R spectrometer (JEOL Ltd., Tokyo, Japan) with a proton frequency of 600 MHz. ^{1}H NMR spectra were acquired in water suppression mode using D_2O as the solvent. Water suppression analysis of products, blanks and standards was done at 128 scans while ^{13}C was done at 20,000 scans.

CHAPTER 4

RESULTS AND DISCUSSION

4.1 Catalyst characterization

The catalyst characterization results provided crucial insights into the physical and chemical properties of the prepared material, which directly influence its performance in methane conversion. The respective results are presented in sections 4.1.1, 4.1.2 and 4.1.3.

4.1.1 X-ray Diffraction

Figure 4.1 shows the X-ray diffraction (XRD) pattern of the synthesized Fe_2O_3 compared with the standard reference pattern of hematite (α-Fe_2O_3). The diffraction peaks of the sample are in excellent agreement with those of hematite from AMCSD 0021163. The key 2θ values observed include 24.1°, 33.2°, 35.6°, 40.8°, 49.4°, 54.0°, 57.6°, and 62.5°, corresponding to the (012), (104), (110), (113), (024), (116), (122), and (214) planes, respectively [75].

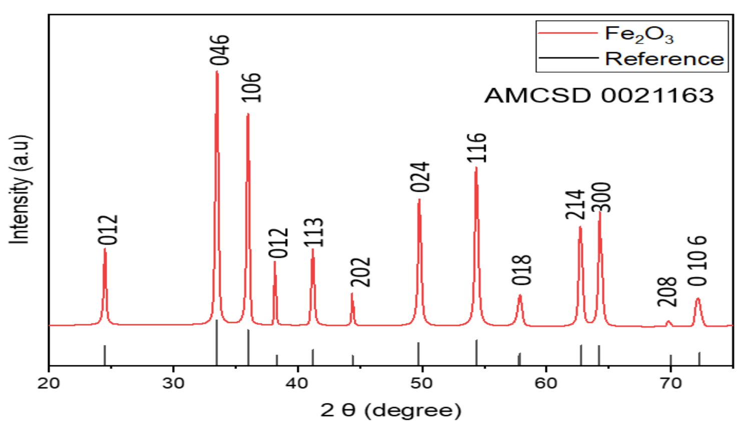

Figure 4.1 XRD pattern of Fe_2O_3 and reference

In Figure 4.2, the XRD profiles of pure Fe_2O_3 (black), graphite felt (red), and Fe_2O_3 coated on graphite (blue) are shown. The graphite sample exhibits a broad peak at ~26° corresponding to the (002) plane of graphite and sharp peaks at 37, 43, 64 and 77° indicative of its layered structure. For the Fe_2O_3-coated graphite composite, the pattern is predominantly governed by the graphite peaks, reflecting its structural dominance since only 5 mg Fe_2O_3 was deposited. Nevertheless, two of the most intense peaks from Fe_2O_3, the peaks at 33 and 36 remain visible, confirming the successful coating onto the graphite surface. The retention of both graphite and a limited amount of Fe_2O_3 peaks suggests that the coating process did not significantly disrupt the graphite structure, making the composite suitable for our applications requiring conductive and catalytic properties.

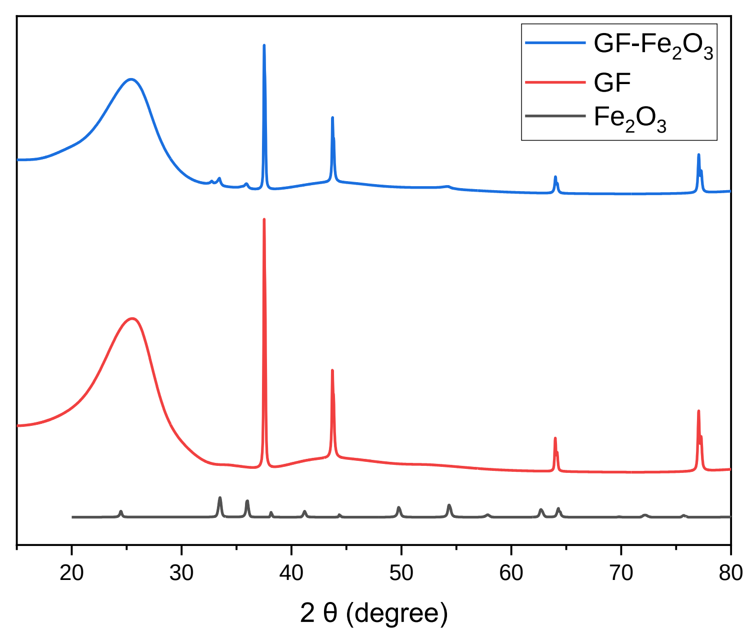

Figure 0.2 XRD Comparison of Fe_2O_3, GF and GF- Fe_2O_3

4.1.2 Scanning Electron Microscopy

Figure 4.3 displays the morphology and elemental composition of Fe_2O_3 as analyzed through scanning electron microscopy (SEM) and energy-dispersive X-ray spectroscopy (EDX). In the SEM images, captured at magnifications corresponding to 500 nm (left) and 1 µm (center), the morphology of Fe_2O_3 appears as a porous agglomeration of nanoparticles. The particles exhibit a relatively uniform size distribution, forming spherical shapes. The increased magnification (500 nm) highlights the granular nature of the material, indicating individual particle sizes in the nanometer range. The smooth surface of the particles shows minimal surface defects. The nanostructure's high surface area provides more active sites suitable for methane oxidation and other catalytic applications [76].

The accompanying EDX spectrum (right) confirms the elemental composition of the sample. Peaks corresponding to Fe constituted about 73 wt % and O consisting of the remaining 27 % the spectrum, confirming the presence of Fe_2O_3. Apart from Fe and O, Au peak was also observed due to a gold coating applied to the sample for SEM imaging to improve conductivity but did not contribute to the composition. The absence of significant peaks for other elements supports the high purity of the material with a clean composition.

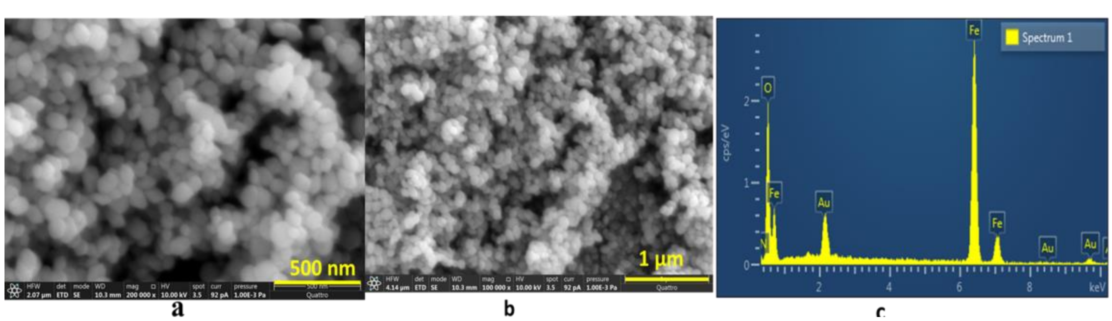

Figure 0.3 SEM images at resolutions of (a) 500 nm (b) 1 µm (c) EDX of of Fe_2O_3

Similarly, we characterized the coated catalyst on the graphite. Figure 4.4 shows the morphology of Fe_2O_3-coated graphite fibers at increasing magnifications (1 µm, 5 µm, 10 µm, and 100 µm), along with the EDX spectrum confirming the elemental composition.

At the 1 µm magnification, small Fe_2O_3 particles are visible as discrete clusters on the surface of the graphite fibers. The particles appear sparsely distributed, consistent with a low coating amount of Fe_2O_3. The smooth underlying texture of the graphite fibers remains evident, suggesting that the coating process preserved the fiber's structure without significant modification. At 10 µm, the overall network of graphite fibers becomes more apparent, with individual fibers maintaining their integrity and showing minimal agglomeration of Fe_2O_3.

The EDX spectrum reveals the elemental composition of the sample, showing prominent peaks for carbon (C) due to the graphite fibers, with smaller peaks for oxygen (O) and iron (Fe), confirming the presence of Fe_2O_3. The weight percentages (C: 92.7%, O: 6.4%, Fe: 0.9%) align with the expected low Fe_2O_3 content. Au peaks were observed as with the Fe_2O_3 only, from the gold sputtering used to enhance conductivity for SEM imaging.

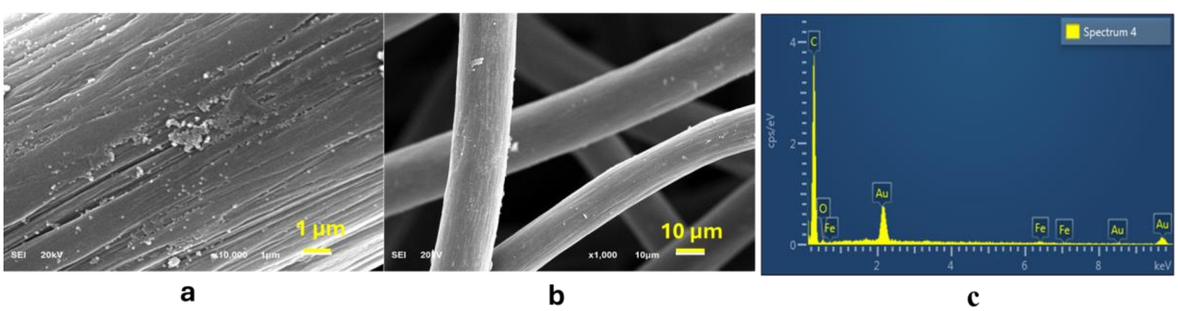

Figure 0.4 SEM images at resolution of (a) 1 µm (b) 10 µm, (c) EDX of for GF-Fe_2O_3

4.1.3 Brunauer-Emmett-Teller

The Brunauer-Emmett-Teller (BET) analysis provides crucial insights into the surface area, pore volume, and pore size of the materials studied, including Fe_2O_3, graphite, and Gf- Fe_2O_3, both before and after reaction. The surface area of Fe_2O_3 was determined to be 125 m^2/g, reflecting the relatively dense structure of the metal oxide, which inherently offers fewer active sites for catalytic reactions. In contrast, graphite exhibited a significantly higher surface area of 366 m^2/g, which can be attributed to its porous, layered structure. This characteristic makes graphite an excellent support material for catalytic applications, as it enhances the dispersion of active sites and promotes accessibility to reactants. Gf- Fe_2O_3 demonstrated a surface area of 339 m^2/g, which is close to that of graphite. This suggests that the integration of Fe_2O_3 with graphite resulted in good dispersion of the metal oxide particles without significantly blocking the pores of the graphite support.

The pore volume data aligns with these observations. Fe_2O_3 exhibited a pore volume of 0.290 cm^3/g, which is typical for dense metal oxides, while graphite showed a much larger pore volume of 0.473 cm^3/g, consistent with its highly porous nature. The GF- Fe_2O_3 composite had an intermediate pore volume of 0.394 cm^3/g, indicating that the incorporation of Fe_2O_3 did not excessively obstruct the pores of the graphite.

The pore size across all samples remained nearly constant, ranging from 1.646 to 1.662 nm. This uniformity suggests that the structural characteristics of the individual materials were largely preserved in the composite and remained stable during the reaction. The pore sizes fall within the mesoporous range (2–50 nm), although they are at the lower end, providing adequate diffusion pathways for reactants and products during the catalytic process. Table 4.1 describes all the details.

Table 0.1 N_2 adsorption desorption before and after coating

Sample	Surface area (m^2/g)	Pore Volume cm^3/g)	Pore size (nm)
Fe_2O_3	124	0.290	1.662
Graphite	366	0.473	1.646
Gf- Fe_2O_3	339	0.394	1.661

4.2 Products detection and analysis

Post-reaction liquid products from electrochemical conversion of methane to methanol in the flow cell setup shown in Figure 3.3 were detected using two complementary techniques: Nuclear Magnetic Resonance (NMR) spectroscopy and Gas Chromatography with Flame Ionization Detection (GC-FID). Analysis of the liquid products and gas is thus discussed in this section.

4.2.1 Gas chromatography with flame ionization detection

Methane oxidation products were analyzed using gas chromatography (GC) with flame ionization detection. Prior to running the experiments, control blanks were measured, which included running water alone, passing oxygen gas instead of methane, and collecting samples from the cathode flask under identical flow cell conditions. Additionally, a sample was taken from the reduction site in the catholyte container. GC chromatograms of these control samples revealed the water peak at ~6.0 minutes consistently observed because the samples all contain water. The results are presented in Figure 4.5 below.

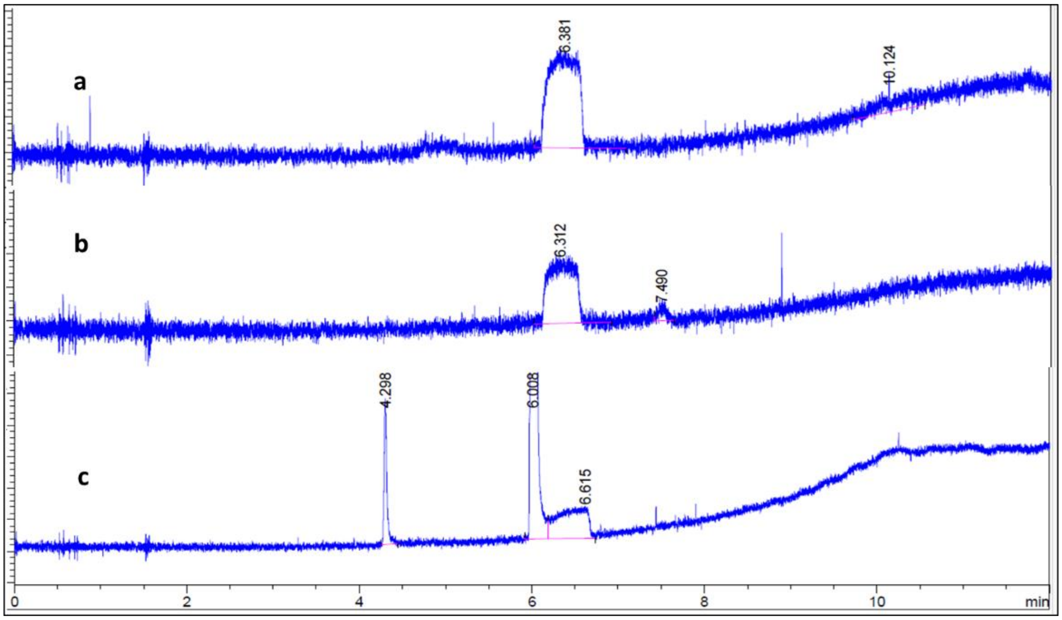

Figure 4.5 Figure 4.5 (a) water (b) O_2 gas instead of methane (c) reduction site sample

Thereafter, commercial standards of the expected products were injected into the GC and well separated. Methanol eluted at approximately 5.2 minutes, ethanol at 5.3 minutes, and a broad water peak appeared around 6.0 minutes as shown in Figure 4.5c. In the reaction with methane only under optimized conditions, methanol was detected with a retention time of about 5.2 minutes as compared by the retention time of the commercial standard. For reactions involving methane and Oxygen gas, methanol and ethanol were identified. Figure 4.6a displays the reaction with methane only, (b) shows the reaction with methane and O_2, and (c) illustrates 10 ppm of methanol and ethanol standards. Here, the detected products were only analyzed, but not quantified. The quantification was done using ^{1}H NMR done in water suppression mode.

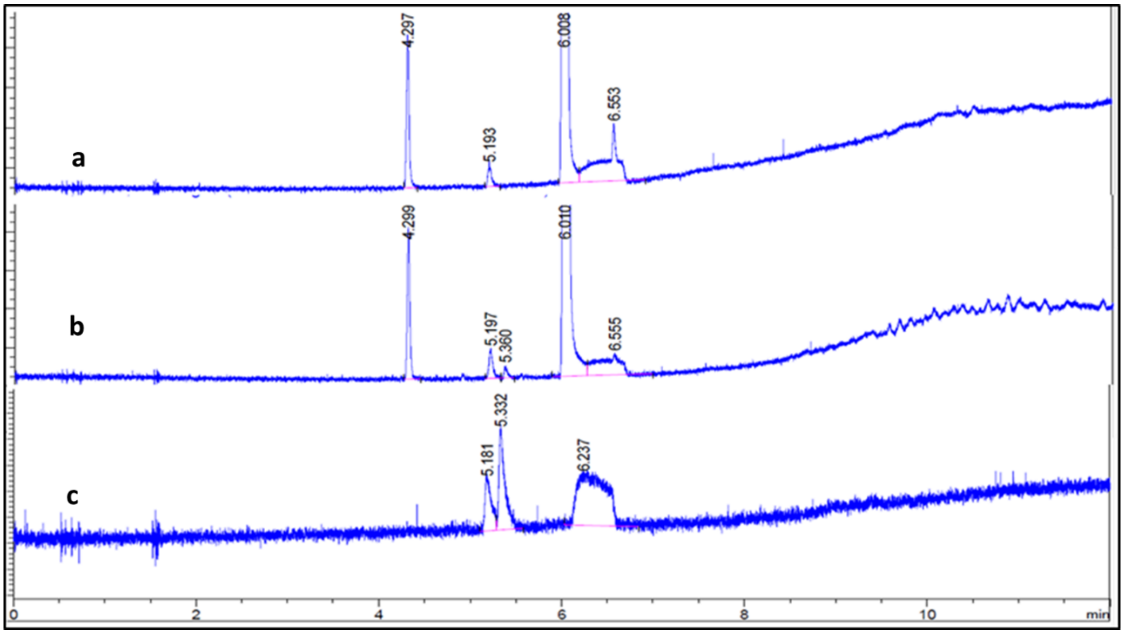

Figure 0.6 GC chromatogram for (a) CH_4 reaction (b) CH_4, O_2 reaction (c) 10 ppm methanol/ethanol standard

After detecting methanol in the sample, gas chromatography was employed to optimize the reaction parameters by analyzing the peak area corresponding to methanol. The optimization study was done to achieve the optimum yield using the most important parameters. These parameters included the reaction time, the pump flow rate, volume of the anolyte solution and the applied voltage. The results are explained in the subsequent sections.

4.2.1.1 Reaction time optimization

The effect of reaction time on product yield was evaluated by monitoring the peak area of methanol in the GC over different durations, as presented in Figure 4.7. At shorter reaction times (10–30 minutes), the yield increases steadily, indicating that the reaction kinetics are still progressing. However, beyond 40 minutes, the rate of improvement diminishes, suggesting that the reaction is nearing completion or equilibrium. The timing was stopped after 60 minutes to report the values in terms of µmol/g/hr. Further reaction time may lead to a slight increase in the retention time. Therefore, the reaction was conducted for 60 minutes, and samples were collected and analyzed accordingly.

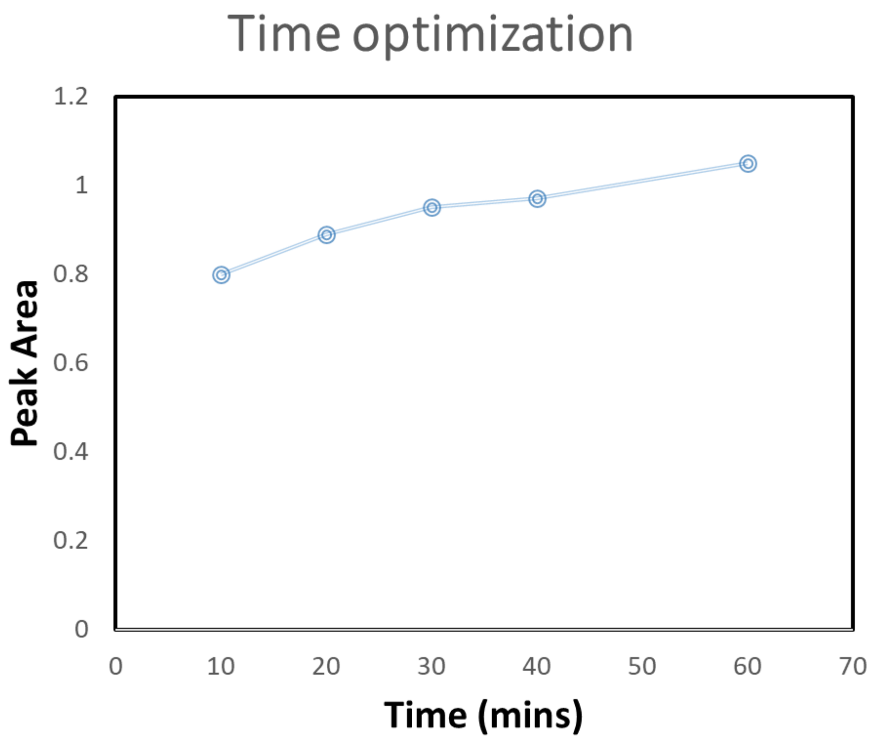

Figure 4.7 Reaction time optimization using methanol peak area from GC-FID

4.2.1.2 Applied potential optimization

The influence of applied voltage on product formation was investigated by measuring the corresponding peak area, as shown in Figure 4.8. The results indicate a significant effect of voltage on catalytic performance within the studied range. An increase in voltage from 0.6 V to 0.9 V led to a progressive rise in peak area, suggesting optimal conditions for product formation at this voltage. Beyond 0.9 V, however, the peak area declined noticeably at 1.0 V and 1.1 V. This reduction is attributed to the onset of competing side reactions at higher voltages. These findings emphasize that 0.9 V is the optimal applied voltage for maximizing product yield in this setup. Consequently, this voltage was applied in subsequent experiments, and the resulting samples were analyzed.

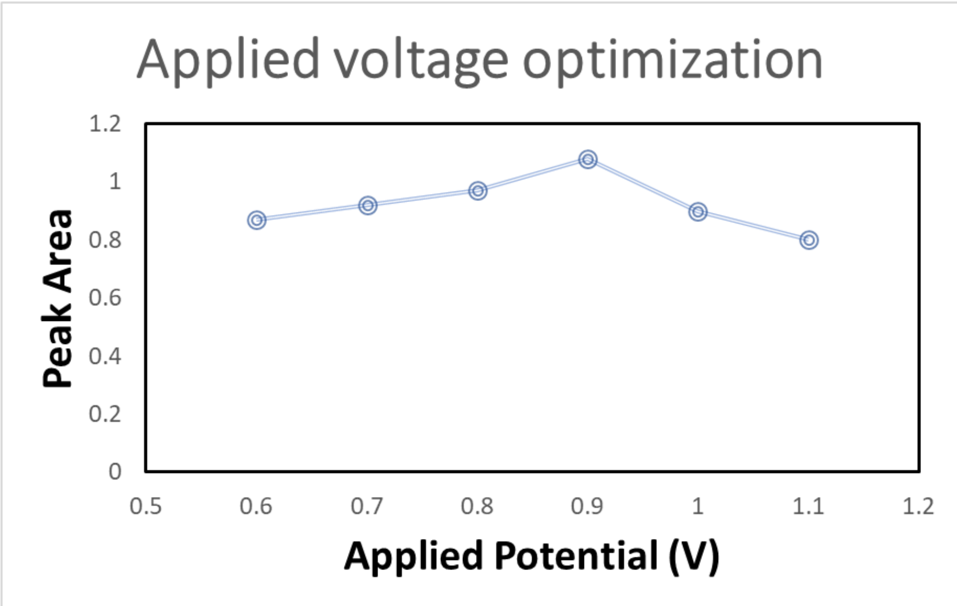

Figure 0.8 Applied voltage optimization using methanol peak area from GC-FID

4.2.1.3 Flow rate optimization

The data shown in Figure 4.9 illustrates the impact of flow rate on the peak area of the products collected during the reaction. As the flow rate increases from 1 mL/min to 5 mL/min, a consistent decline in the peak area is observed. The highest peak area is recorded at a flow rate of 1 mL/min, while the lowest is seen at 5 mL/min. At lower flow rates, the reactants have a longer residence time over the catalyst bed, allowing for more effective contact and reaction on the catalyst's surface. As the flow rate increases, the reduced residence time limits the interaction of methane with the catalyst, thereby reducing the amount of product formed or collected. Additionally, higher flow rates may dilute the concentration of the products, leading to lower peak areas in the chromatogram. This trend highlights the importance of optimizing the flow rate for maximum product yield. A flow rate of 1–2 mL/min represents the optimal range for this system, balancing both efficiency and throughput. As a result, this flow rate was adopted for subsequent analyses.

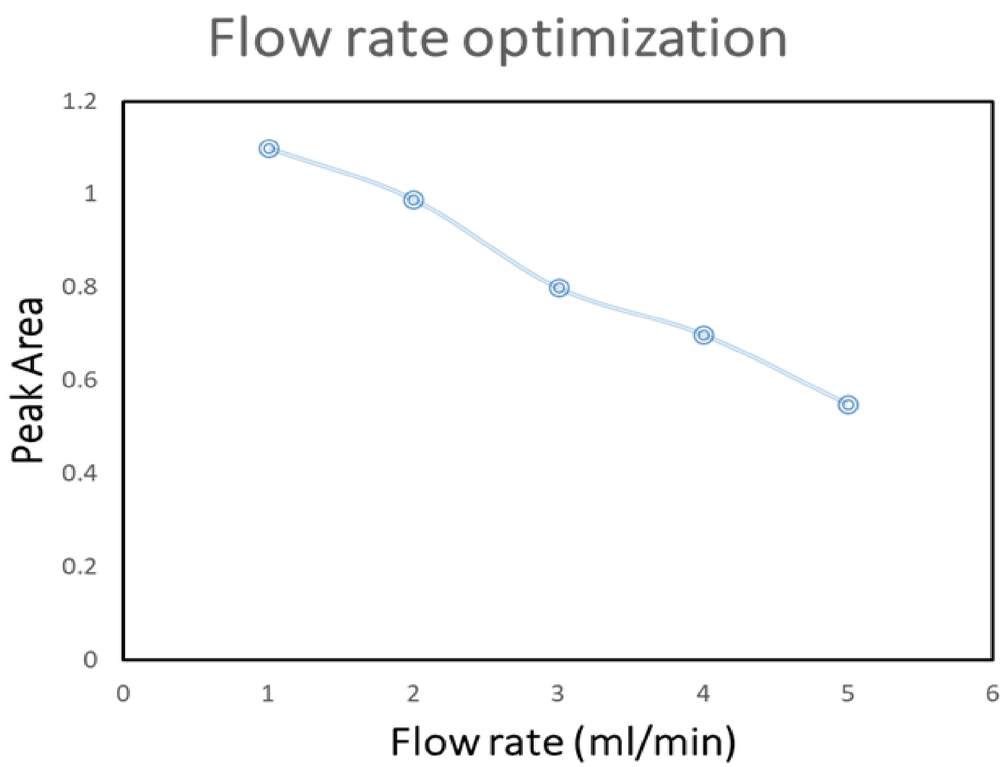

Figure 0.9 Flow rate optimization using methanol peak area from GC-FID

4.2.1.4 Electrolyte volume optimization

The relationship between electrolyte volume and peak area was evaluated to determine the optimal operating conditions for the reaction system, as shown in Figure 4.8. The results demonstrate that an electrolyte volume of 15 mL yielded the highest peak area, indicating the maximum product formation. This volume also represents the minimum required to ensure continuous flow in the experimental setup, supporting steady-state reaction conditions. At volumes above 20 mL, a decline in peak area was observed. This decrease may result from the dilution of reactants within the electrolyte, reducing their availability for the catalytic reaction. Additionally, higher volumes could affect the flow dynamics, potentially disrupting efficient interaction between the methane gas, catalyst, and electrolyte. The study establishes 20 mL as the critical volume to balance the need for continuous flow and optimal catalytic activity, ensuring efficient product formation in the system. Therefore, this volume was maintained in all further experiments.

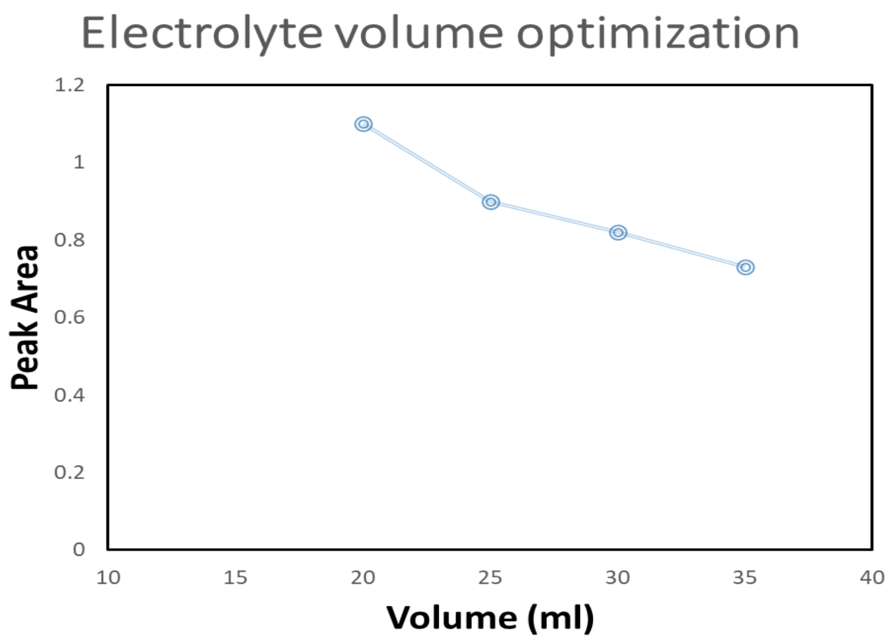

Figure 0.10 Electrolyte volume optimization using methanol peak area from GC-FID

4.2.2 Nuclear Magnetic Resonance (NMR)

The liquid products from methane oxidation were further analyzed by NMR. For each analysis, 0.5 mL of post-reaction sample was combined 0.1 mL of a dimethyl sulfoxide (DMSO) internal standard solution (10 ppm) and with 0.1 mL D_2O. A calibration curve was generated by plotting the concentration of the standard product solution against the integrated areas of the product and DMSO signals. Product quantification was achieved by comparing the ^1H NMR signal with this calibration curve. The calibration curves for methanol and ethanol are shown in Figure 4.11 below.

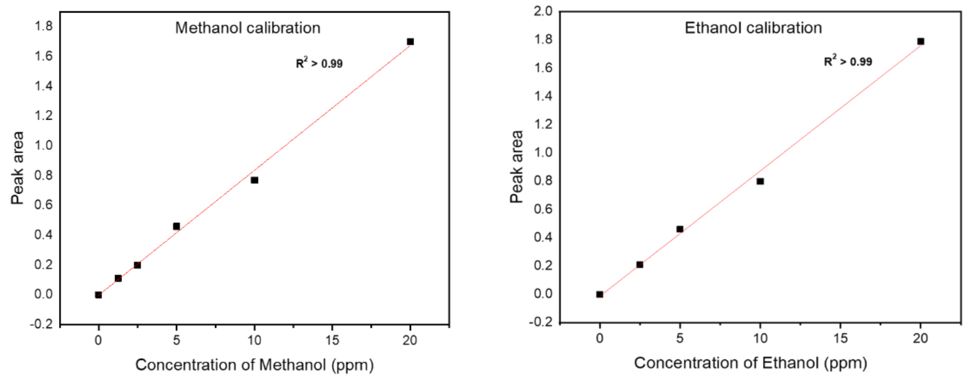

Figure 4.11 Methanol and ethanol calibration

4.2.2.1 Water suppression mode NMR

Like the GC analysis of the blank experiments, the ^1H NMR spectrum of the control samples showed no peaks associated with methanol, ethanol, acetic acid, or formic acid, with only the residual peak of D_2O observed at 4.7 ppm. These findings, illustrated in Figure 4.12, indicate that the detected products originated from methane oxidation reactions.

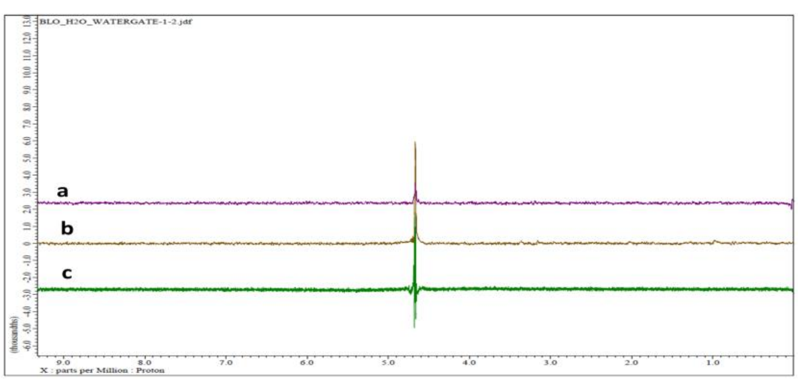

Figure 4.12 NMR for (a) water (b) reduction side product (c) reaction with O_2

Thereafter, post reaction samples were analyzed. In the reaction with optimized condition and methane alone, the ^{1}H NMR shows a singlet at 3.2 ppm corresponding to the methyl protons of methane, the OH were exchanged by D_2O and the residual D_2O peak was at 4.7 ppm. In the reactions involving methane + O_2, methanol and ethanol were detected. These are shown in Figure 4.13.

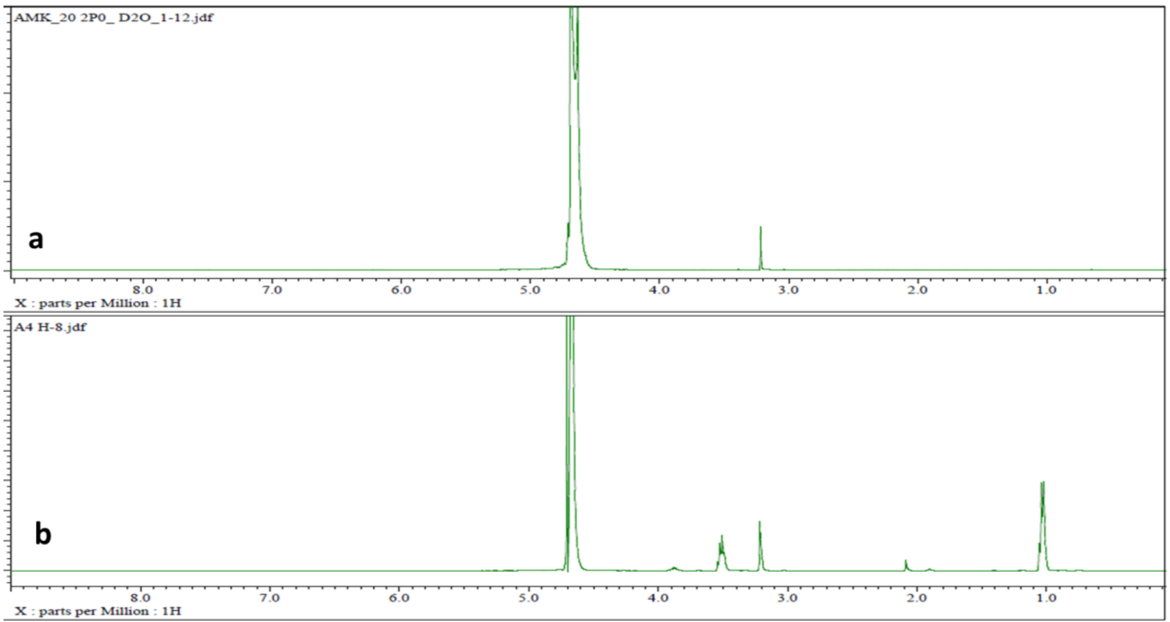

Figure 0.13 NMR of (a) methane (b) methane and O_2

4.2.2.2 Carbon-13 Nuclear Magnetic Resonance

The ^{13}C NMR spectra in Figure 4.14 provide complementary insights to proton NMR regarding the carbon-based products from methane oxidation. Spectrum (a), obtained under optimized conditions using methane alone, shows a single peak at 49 ppm, corresponding to the carbon in methanol, confirming selective oxidation of methane to methanol. Spectrum (b), representing the reaction with methane and oxygen, similarly shows a peak at 49 ppm for methanol but also features two additional peaks at 17 ppm and 58 ppm, corresponding to the methyl and methylene carbons in ethanol respectively. These additional peaks indicate that the presence of oxygen facilitates further oxidation pathways, enabling ethanol formation alongside methanol.

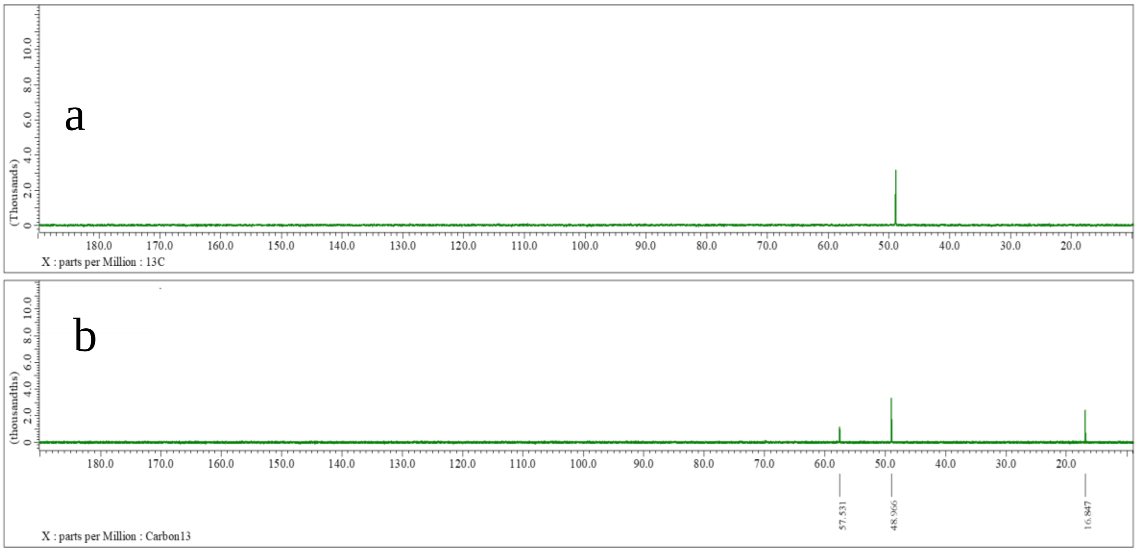

Figure 4.14 ^{13}C NMR Spectra of Reaction Products for (a) Methane Oxidation Under Optimized Conditions and (b) Methane/Oxygen System

4.2.3 Improvement of yield with the use of KCl

The addition of KCl as an electrolyte significantly enhanced the yield of methanol in the reaction system. The enhancement in methanol yield observed can be attributed to several electrochemical mechanisms. The increased ionic strength and conductivity provided by KCl lower the resistance of the electrolyte, improving charge transfer efficiency and enabling more effective catalysis. Cl^- ions may also adsorb onto the catalyst surface, stabilizing its active sites and preventing deactivation, thereby sustaining catalytic activity and enhancing selectivity towards methanol. Furthermore, the presence of Cl^- likely promotes methane solubility in the aqueous electrolyte through weak interactions, ensuring a higher local concentration of methane at the electrode surface and improving its availability for oxidation [77]. These mechanisms collectively provide a plausible explanation for the improved methanol yield in my system, demonstrating how the unique properties of Cl^- ions can optimize electrocatalytic performance.

Post reaction samples were then transferred to NMR tubes and analyzed for water suppression. Figure 4.15 shows the NMR of the reaction of CH_4 under optimized condition using KCl solution and water.

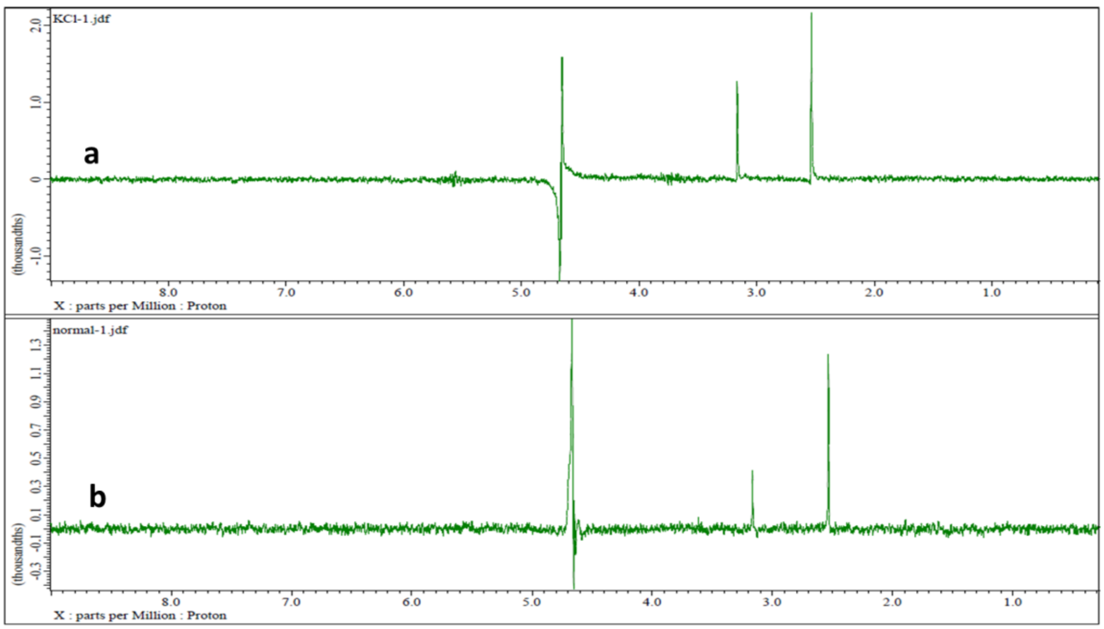

Figure 0.15 NMR of products of CH_4 reaction using (a) KCl solution (b) water as electrolytes

The reaction of methane under optimized condition using KCl as electrolytes was also analyzed in the GC-FID. However, because salts are not suitable with the GC column, we used SPME to adsorb the products on the fiber followed by desorbing manually in the GC injector. The SPME set up is shown in Figure 4.16. After 20 minutes of extraction, the fiber was injected, and the components were separated. The chromatograms in Figure 4.17 show the methanol peak at about 5.2 minutes retention time for the optimized conditions and reacting with methane using KCl as electrolyte.

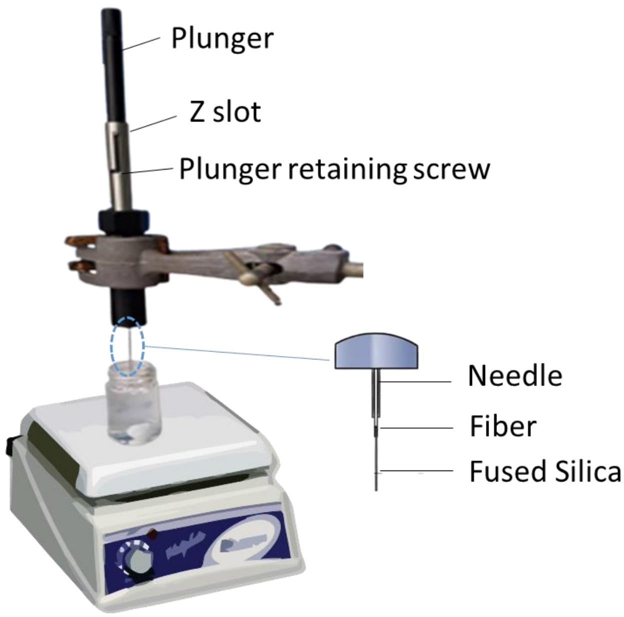

Figure 4.16 Solid Phase Microextraction

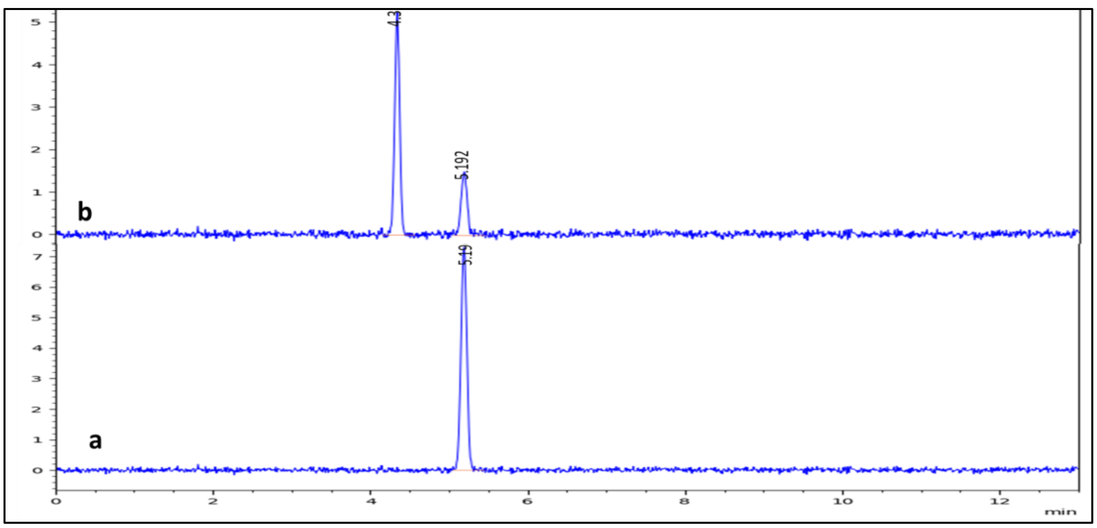

Figure 4.17 GC-FID of SPME for (a) CH_4 reaction using KCl (b) standard methanol

4.2.4 Gas products analysis

Methane conversion produces gases in addition to liquid products, therefore, gas was collected in an airbag and injected into a gas chromatography coupled with flame ionization detection. The chromatogram shows the peak of CO_2 at about 1 minute, Hydrogen at 10 minute and methane at around 13 minutes and an additional peak in less than 1 minute due to purging the gas. The chromatogram is shown in Figure 4.18.

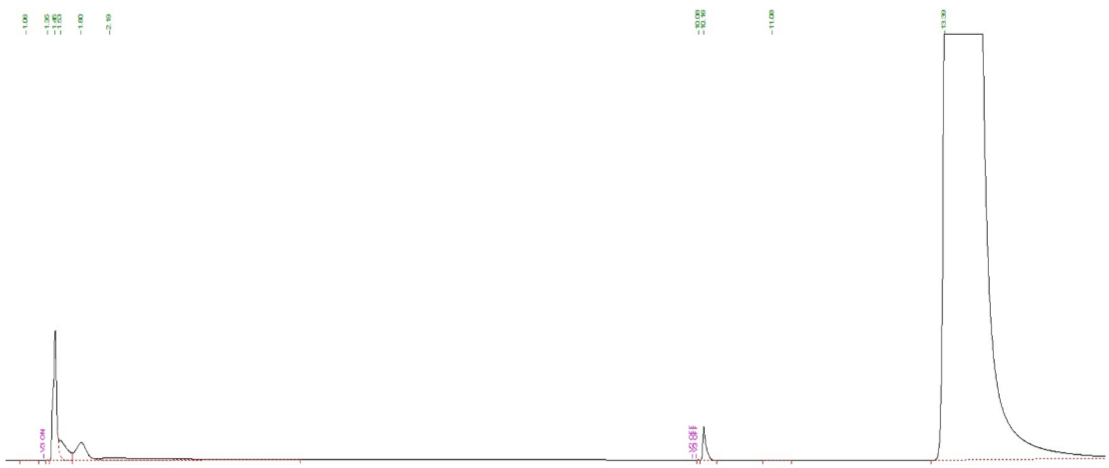

Figure 4.18 GC-TCD of gas samples

4.3 Proposed mechanism for methane to methanol oxidation

4.3.1 Methane to methanol using water

Methane oxidation with water as oxidant takes place at the anode of the electrochemical cell [78]. The first step involves creation of an adsorbed OH^- group, which subsequently undergoes dehydrogenation to generate an O* as shown in Equations 3 and 4. The second stage involves reaction between adsorbed active species with methane to produce methanol as shown in Equation 3. A lower energy requirement for each step suggests that the step is more likely to occur, which means a reduced minimum anode potential is necessary for the reaction to advance. To achieve high selectivity to methanol, it is necessary to avoid the formation of CH_3O* and CH_3*. CH_3O* cannot be reduced to CH_3OH* under anodic conditions because CH_3* is susceptible to further oxidation to form CH_2*, CH*, and C*, which can result in the formation of unwanted by-products such as HCHO, CO, and CO_2 [54].

$$M* + 2H_2O \rightarrow *OH + H_2O + H^+ + e^- \quad (3)$$

$$*OH + H_2O \rightarrow *O + H_2O + H^+ + e^- \quad (4)$$

$$*O + CH_4 \rightarrow *O\text{---}CH_4 \rightarrow *(O\text{---}CH_3) \rightarrow *CH_3OH \rightarrow CH_3OH \quad (5)$$

M* indicates the surface of the catalyst.

4.3.2 Methane oxidation using Potassium Chloride

The mechanism was adopted for our study involving methane bubbling through salt water to achieve methane conversion to methanol (accepted for publication) [77]. The Cl• is the major activation radical, and the GF-Fe_2O_3 electrode serves as an anode to remove an electron from Cl^- to generate reactive Cl• (Equation 6). Cl• reacts with CH_4 to generate CH_3• (Equation 7) and liberate in solution H^+ and Cl^-. At the same time, at the GWI, OH^- loses an electron to form the OH• radical (Equation 8), which recombines with CH_3• to form methanol (Equation 9). Overall, the sum of these steps is shown in Equation 10.

$$Cl^- \rightarrow Cl\bullet + e^- \quad (6)$$

$$Cl\bullet + CH_4 \rightarrow CH_3\bullet + HCl\,(H^+ + Cl^-) \quad (7)$$

$$OH^- \rightarrow OH\bullet + e^- \quad (8)$$

$$CH_3\bullet + OH\bullet \rightarrow CH_3OH \quad (9)$$

$$CH_4 + OH^- \rightarrow CH_3OH + H^+ + 2e^- \quad (10)$$

4.4 Performance Results

This section evaluates the effectiveness of the electrocatalytic methane oxidation process, focusing on key performance metrics: conversion, which measures the proportion of methane reacted; yield, which quantifies the amount of methanol produced relative to the theoretical maximum; and selectivity, which indicates the preference of the reaction towards methanol over other by-products. Together, these metrics provide a comprehensive assessment of the reaction's efficiency and optimization potential.

4.4.1 Conversion

Conversion refers to the percentage of methane molecules transformed into the products, such as methanol, formic acid, or CO_2. It is a critical metric for evaluating the efficiency of the reaction and the catalyst, calculated as the ratio of methane consumed to the total methane supplied. The formula used for this calculation is presented in Equation 11.

$$Conversion = \frac{CH_4,reacted}{nCH_4,in} \ x\ 100\ \% \qquad 11$$

nCH_4, in: Initial moles of methane (fed into the system)

nCH_4, reacted = nCH_3OH +nCO_2

4.4.2 Selectivity

Selectivity is a critical parameter in methane conversion, defining the proportion of methane that is transformed into the desired product relative to all products formed during the reaction. High methanol selectivity ensures that the reaction predominantly yields methanol while minimizing the formation of other liquid products. The formula used is shown in Equation 12.

$$Methanol\ selectivity = \frac{n\ CH_3OH}{n\ total\ oxygenates} x\ 100\% \qquad 12$$

4.4.3 Methanol Yield

The yield of methanol in methane conversion refers to the amount of methanol produced per gram of catalyst per hour, typically expressed in µmol/g.hr. This metric is crucial for evaluating the efficiency and productivity of the catalyst in converting methane into methanol. High yield indicates that a significant amount of methane is successfully transformed into methanol in one hour, demonstrating the catalyst's effectiveness. The formula used for the yield calculation is shown in Equation 13.

$$Product\left(\frac{\mu mol}{g_{cat}}\right) = \frac{n\ products}{g_{cat}} \quad 13$$

4.4.4 Performance summary

The results highlight the significant impact of electrolyte composition and reactants on methane oxidation. Using H_2O as the electrolyte achieves 37% methane conversion with a methanol yield of 873 µmol/g/hr and 100% selectivity. Adding 3% KCl improves conversion to 49% and boosts methanol yield to 1248 µmol/g/hr, maintaining 100% selectivity. In contrast, introducing O_2 with H_2O as the electrolyte increases methane conversion to 44% but reduces methanol selectivity to 62%, producing additional by-products such as ethanol. While O_2 enhances conversion, it complicates product distribution, whereas 3% KCl gave the most effective for achieving high methanol yield and selectivity.

Table 4.2 Performance Summary of Electrocatalytic Methane Oxidation Reactions Investigated in This Study

Reactants	**Electrolyte**	**CH_4 conversion %**	**Products**	**Methanol Selectivity**	**Yield µmol/g/hr**
CH_4	H_2O	37	CH_3OH	100	873
CH_4	3% KCl	49	CH_3OH	100	1248
CH_4, O_2	H_2O	44	CH_3OH, CH_3CH_2OH	62	998

4.4.5 Result comparison

This table compares the performance of various catalysts and setups for methane oxidation, focusing on conversion, selectivity, yield, and operating conditions. In your work, Fe_2O_3 was employed as the catalyst in a two-electrode flow cell with KCl as the electrolyte, operating at room temperature (RT). This setup achieved a conversion of 49% and a remarkable 100% selectivity to methanol (CH_3OH) with a yield of 1248 μmol/g/hr.

In comparison, Fe_2O_3 and Zr-Fe_2O_3 were tested in three-electrode cells with Na_2CO_3 electrolyte, also at RT, yielding higher conversions of 87%. However, these setups produced multiple products, including methanol, ethanol and acetone with the highest selectivity of 90.5% to ethanol for Zr-Fe_2O_3. Although the yields were higher for ethanol production (1677 μmol/g/hr for Zr-Fe_2O_3 and 1198 μmol/g/hr for Fe_2O_3, the presence of mixed products requires additional separation steps, reducing the overall efficiency for pure methanol synthesis.

A further comparison can be made with V_2O_5/SnO_2 coated with PTFE, which operated in a two-electrode cell with water as the electrolyte at an elevated temperature of 100°C. This system achieved an 88% conversion and a selectivity of 88.4% to methanol. While the conversion and selectivity are competitive, the higher operating temperature increases energy consumption compared to your RT system. Our system demonstrates a balance of moderate conversion, excellent selectivity, and reasonable yield under the simplest and mildest conditions. This makes it a promising approach for energy-efficient and selective methanol production, especially in applications prioritizing purity and low-energy processes.

Table 0.3 Comparative Performance Analysis of Methane Oxidation: Results from This Study and Relevant Literature

Cell type	**Catalyst**	**Electrolyte**	**Temperature (° C)**	**Conversion (%)**	**Products**	**Selectivity (%)**	**Yield µmol/g/hr**	**Ref.**
Flow cell Two electrodes cell (PEM)	Fe_2O_3	KCl	RT	49	CH_3OH	100 CH_3OH	1248	This work
Three electrodes cell	Fe_2O_3	Na_2CO_3	RT	87	CH_3OH CH_3CH_2OH CH_3COCH_3	86.1 CH_3CH_2OH	1198 CH_3CH_2OH	[67]
Three electrodes cell	Zr-Fe_2O_3	Na_2CO_3	RT	87	CH_3OH CH_3CH_2 CH_3COCH_3	90.5 CH_3CH_2OH	1677 CH_3CH_2OH	[67]
Two electrode cells (PEM)	V_2O_5/SnO_2;PTFE	H_2O	100	88	CH_3OH	88.4 CH_3OH	-	[61]

CHAPTER 5

SUMMARY AND CONCLUSION

5.1 SUMMARY

This thesis explored the potential of electrocatalytic methane conversion to methanol using Fe_2O_3-based catalysts, presenting a dual benefit of mitigating methane's environmental impact while generating a valuable platform chemical. Employing a flow cell system operating at room temperature, the study demonstrated how optimized reaction parameters could improve selectivity, yield, and conversion efficiency.

Key findings include the successful synthesis and characterization of highly pure, porous Fe_2O_3 catalysts through techniques including XRD, SEM, and BET. These catalysts, integrated onto graphite supports, preserved the graphite's high surface area and conductivity while enhancing catalytic activity.

The research utilized a flow cell reactor divided by Nafion 117, a proton exchange membrane, with water serving as the oxidant. Post-reaction samples were analyzed using gas chromatography with flame ionization detection (GC-FID) and nuclear magnetic resonance (NMR) spectroscopy, enabling precise detection and quantification of reaction products. ^{13}C NMR was used to confirm the results of ^{1}H NMR. The GC peak area for methanol was instrumental in optimizing the influence of reaction parameters, including applied voltage, flow rate, and electrolyte composition, on performance metrics. The results demonstrated that optimal conditions—including a reaction time of one hour, a flow rate of 1 mL/min, and an applied voltage of 0.9 V—resulted in methanol yields of up to

873 μmol/g/hr with 100% selectivity. Quantification of the products was achieved using 1H NMR with DMSO as an internal standard, supported by linear calibration curves for the detected products.

A notable enhancement was observed with the use of potassium chloride (KCl) as an electrolyte. The chloride ions facilitated improved methane solubility and charge transfer efficiency, boosting methanol yield to 1248 μmol/g/hr while maintaining full selectivity. Comparative analysis with existing technologies highlighted the advantages of the developed system, which operates under ambient conditions and eliminates the need for energy-intensive processes, offering a cost-effective and environmentally friendly alternative.

5.2 CONCLUSION

The study successfully demonstrated that Fe_2O_3-coated on graphite catalysts could facilitate the selective conversion of methane to methanol at room temperature with minimal environmental impact. Key findings include:

1. Catalyst Synthesis and Characterization: The synthesis and detailed characterization of Fe_2O_3 and Fe_2O_3-coated graphite catalysts revealed their suitability for methane oxidation. The nanostructured Fe_2O_3 provided high surface areas and abundant active sites, while the graphite substrate offered superior conductivity and structural stability, essential for sustained catalytic performance.

2. Reaction Optimization and Performance: Systematic optimization of reaction parameters significantly enhanced catalytic efficiency. The study identified optimal conditions for applied voltage, flow rate, and electrolyte composition, achieving

maximum methanol yield and selectivity. The ability to fine-tune these parameters highlights the system's adaptability for various operational requirements.

3. Electrolyte Innovation: The inclusion of KCl as an electrolyte proved transformative, addressing challenges related to methane solubility and catalyst activity. Chloride ions enhanced the reaction environment, stabilized active sites, and prevented catalyst deactivation, collectively contributing to the highest methanol yield reported in this study.

4. Comparison with Alternative Systems: Comparative analysis underscored the system's advantages over traditional H-cell and proton exchange membrane (PEM) systems. While H-cells demonstrated higher conversion rates, the flow cell design employed here uniquely achieved 100% methanol selectivity with no detectable by-products, emphasizing its value for simplified downstream processing and industrial applicability.

5. Environmental Relevance: Operating under ambient conditions, the system minimizes energy consumption and environmental impact, addressing the sustainability concerns associated with conventional methane conversion methods.

5.3 RECOMMENDATION

1. Detailed Reaction Mechanisms: Future research must focus on clarifying the reaction mechanisms involved in the conversion of methane to methanol. A thorough comprehension of these mechanisms is crucial for optimizing catalyst performance and improving both selectivity and efficiency.

2. Broader Conversion Pathways: There is potential to broaden research efforts towards the direct transformation of methane into various liquid fuels or chemicals, including ethanol and acetic acid, thereby expanding the range of possible applications.
3. Greenhouse Gas Utilization: Similar electrocatalytic approaches could be employed to convert other greenhouse gases, such as carbon dioxide, into valuable products, thereby playing a significant role in climate change mitigation strategies.
4. Catalyst Enhancement: Investigating the doping of Fe_2O_3 with various elements or the integration of additional materials could lead to significant improvements in catalytic activity, stability, and resistance.

REFERENCE

[1] A. Kaur, A. Tanwar, H. Kaur, and J. Singh, "A Study on Linkage between Global Warming Indicators and Climate Change Expenditure," *IOP Conf Ser Earth Environ Sci*, vol. 1110, no. 1, pp. 0–18, 2023, doi: 10.1088/1755-1315/1110/1/012059.

[2] P. Promoppatum and V. Viswanathan, "Identifying Material and Device Targets for a Flare Gas Recovery System Utilizing Electrochemical Conversion of Methane to Methanol," *ACS Sustain Chem Eng*, vol. 4, no. 3, pp. 1736–1745, Mar. 2016, doi: 10.1021/acssuschemeng.5b01714.

[3] M. A. Mehrgardi, M. Mofidfar, and R. N. Zare, "Sprayed Water Microdroplets Are Able to Generate Hydrogen Peroxide Spontaneously," *J Am Chem Soc*, vol. 144, no. 17, pp. 7606–7609, May 2022, doi: 10.1021/jacs.2c02890.

[4] D. T. Shindell, J. S. Fuglestvedt, and W. J. Collins, "The social cost of methane: theory and applications," *Faraday Discuss*, vol. 200, pp. 429–451, 2017, doi: 10.1039/C7FD00009J.

[5] IEA, "Methane Tracker 2021. International Energy Agency," https://www.iea.org/reports/methane-tracker-2021.

[6] T. K. Wood, I. Gurgan, E. T. Howley, and I. H. Riedel-Kruse, "Converting methane into electricity and higher-value chemicals at scale via anaerobic microbial fuel cells," *Renewable and Sustainable Energy Reviews*, vol. 188, p. 113749, Dec. 2023, doi: 10.1016/j.rser.2023.113749.

[7] K. A. Mar, C. Unger, L. Walderdorff, and T. Butler, "Beyond CO2 equivalence: The impacts of methane on climate, ecosystems, and health," *Environ Sci Policy*, vol. 134, pp. 127–136, Aug. 2022, doi: 10.1016/j.envsci.2022.03.027.

[8] O. Schneising, M. Buchwitz, M. Reuter, S. Vanselow, H. Bovensmann, and J. P. Burrows, "Remote sensing of methane leakage from natural gas and petroleum systems revisited," *Atmos Chem Phys*, vol. 20, no. 15, pp. 9169–9182, 2020, doi: 10.5194/acp-20-9169-2020.

[9] "US. Environmental Protection Agency (2023). Inventory of U.S. Greenhouse Gas Emissions and Sinks: 1990-2021."

[10] D. Sheldon, "Methanol Production - A Technical History," *Johnson Matthey Technology Review*, vol. 61, no. 3, pp. 172–182, Jul. 2017, doi: 10.1595/205651317X695622.

[11] X. Zhang, R. Liu, T. Liu, C. Pei, and J. Gong, "Redox catalysts for chemical looping methane conversion," *Trends Chem*, vol. 5, no. 7, pp. 512–525, Jul. 2023, doi: 10.1016/j.trechm.2023.03.001.

[12] N. Salahudeen, A. A. Rasheed, A. Babalola, and A. U. Moses, “Review on technologies for conversion of natural gas to methanol,” *J Nat Gas Sci Eng*, vol. 108, p. 104845, Dec. 2022, doi: 10.1016/j.jngse.2022.104845.

[13] S. Abernethy, M. I. Kessler, and R. B. Jackson, “Assessing the potential benefits of methane oxidation technologies using a concentration-based framework,” *Environmental Research Letters*, vol. 18, no. 9, p. 094064, Sep. 2023, doi: 10.1088/1748-9326/acf603.

[14] Y. Xu *et al.*, “Regulating Au coverage for the direct oxidation of methane to methanol,” *Nat Commun*, vol. 15, no. 1, p. 564, Jan. 2024, doi: 10.1038/s41467-024-44839-6.

[15] A. Indarto, “A review of direct methane conversion to methanol by dielectric barrier discharge,” *IEEE Transactions on Dielectrics and Electrical Insulation*, vol. 15, no. 4, pp. 1038–1043, 2008, doi: 10.1109/TDEI.2008.4591225.

[16] K. Cheng *et al.*, “Advances in Catalysis for Syngas Conversion to Hydrocarbons,” 2017, pp. 125–208. doi: 10.1016/bs.acat.2017.09.003.

[17] H. Soucie, M. Elam, and W. E. Mustain, “Practical Assessment for At-Scale Electrochemical Conversion of Methane to Methanol,” *ACS Energy Lett*, vol. 8, no. 2, pp. 1218–1229, Feb. 2023, doi: 10.1021/acsenergylett.2c02586.

[18] A. Bakhtyari, M. Parhoudeh, and M. R. Rahimpour, “Optimal conditions in converting methanol to dimethyl ether, methyl formate, and hydrogen utilizing a double membrane heat exchanger reactor,” *J Nat Gas Sci Eng*, vol. 28, pp. 31–45, Jan. 2016, doi: 10.1016/j.jngse.2015.11.028.

[19] A. and K. J. V. Standen, “Alcohols and their derivatives.” Oct. 11, 2024.

[20] M. J. Da Silva, “Synthesis of methanol from methane: Challenges and advances on the multi-step (syngas) and one-step routes (DMTM),” *Fuel Processing Technology*, vol. 145, pp. 42–61, 2016, doi: 10.1016/j.fuproc.2016.01.023.

[21] N. F. Dummer *et al.*, “Methane Oxidation to Methanol,” *Chem Rev*, vol. 123, no. 9, pp. 6359–6411, May 2023, doi: 10.1021/acs.chemrev.2c00439.

[22] S. Yuan *et al.*, “Conversion of Methane into Liquid Fuels—Bridging Thermal Catalysis with Electrocatalysis,” *Adv Energy Mater*, vol. 10, no. 40, pp. 1–19, 2020, doi: 10.1002/aenm.202002154.

[23] B. Wang, S. Albarracín-Suazo, Y. Pagán-Torres, and E. Nikolla, “Advances in methane conversion processes,” *Catal Today*, vol. 285, pp. 147–158, 2017, doi: 10.1016/j.cattod.2017.01.023.

[24] W. Wang *et al.*, “Selective Oxidation of Methane to Methanol over Au/H-MOR,” *J Am Chem Soc*, vol. 145, no. 23, pp. 12928–12934, Jun. 2023, doi: 10.1021/jacs.3c04260.

[25] S. J. Freakley, N. Dimitratos, D. J. Willock, S. H. Taylor, C. J. Kiely, and G. J. Hutchings, “Methane Oxidation to Methanol in Water,” *Acc Chem Res*, vol. 54, no. 11, pp. 2614–2623, Jun. 2021, doi: 10.1021/acs.accounts.1c00129.

[26] I. N. Tsimpanogiannis, I. G. Economou, and A. K. Stubos, “Methane solubility in aqueous solutions under two-phase (H–Lw) hydrate equilibrium conditions,” *Fluid Phase Equilib*, vol. 371, pp. 106–120, Jun. 2014, doi: 10.1016/j.fluid.2014.03.012.

[27] M. Zhong *et al.*, “Engineering PdAu Nanowires for Highly Efficient Direct Methane Conversion to Methanol under Mild Conditions,” *The Journal of Physical Chemistry C*, vol. 125, no. 23, pp. 12713–12720, Jun. 2021, doi: 10.1021/acs.jpcc.1c04252.

[28] T. Moteki, N. Tominaga, and M. Ogura, “CO-Assisted Direct Methane Conversion into C_1 and C_2 Oxygenates over ZSM-5 Supported Transition and Platinum Group Metal Catalysts Using Oxygen as an Oxidant,” *ChemCatChem*, vol. 12, no. 11, pp. 2957–2961, Jun. 2020, doi: 10.1002/cctc.202000168.

[29] M. R. A. Kishore, S. Lee, and J. S. Yoo, “Fundamental Limitation in Electrochemical Methane Oxidation to Alcohol: A Review and Theoretical Perspective on Overcoming It,” *Advanced Science*, vol. 10, no. 31, Nov. 2023, doi: 10.1002/advs.202301912.

[30] S. A. Vali, A. A. Markeb, J. Moral-Vico, X. Font, and A. Sánchez, “Recent Advances in the Catalytic Conversion of Methane to Methanol: From the Challenges of Traditional Catalysts to the Use of Nanomaterials and Metal-Organic Frameworks,” *Nanomaterials*, vol. 13, no. 20, p. 2754, Oct. 2023, doi: 10.3390/nano13202754.

[31] B. Wang, S. Albarracín-Suazo, Y. Pagán-Torres, and E. Nikolla, “Advances in methane conversion processes,” *Catal Today*, vol. 285, pp. 147–158, May 2017, doi: 10.1016/j.cattod.2017.01.023.

[32] M. Kaur, Z. Li, S. Meng, W. Li, and H. Song, “Electrocatalytic methane conversion to high value chemicals at ambient conditions,” *Energy Convers Manag*, vol. 285, p. 117029, Jun. 2023, doi: 10.1016/j.enconman.2023.117029.

[33] J. A. Arminio-Ravelo and M. Escudero-Escribano, “Strategies toward the sustainable electrochemical oxidation of methane to methanol,” *Curr Opin Green Sustain Chem*, vol. 30, p. 100489, Aug. 2021, doi: 10.1016/j.cogsc.2021.100489.

[34] X. Meng, X. Cui, N. P. Rajan, L. Yu, D. Deng, and X. Bao, “Direct Methane Conversion under Mild Condition by Thermo-, Electro-, or Photocatalysis,” *Chem*, vol. 5, no. 9, pp. 2296–2325, Sep. 2019, doi: 10.1016/j.chempr.2019.05.008.

[35] B. Lee and T. Hibino, “Efficient and selective formation of methanol from methane in a fuel cell-type reactor,” *J Catal*, vol. 279, no. 2, pp. 233–240, Apr. 2011, doi: 10.1016/j.jcat.2010.12.020.

[36] R. S. Rocha, R. M. Reis, M. R. V. Lanza, and R. Bertazzoli, “Electrosynthesis of methanol from methane: The role of V2O5 in the reaction selectivity for methanol of a TiO2/RuO2/V2O5 gas diffusion electrode,” *Electrochim Acta*, vol. 87, pp. 606–610, Jan. 2013, doi: 10.1016/j.electacta.2012.09.113.

[37] L. Arnarson *et al.*, “Fundamental limitation of electrocatalytic methane conversion to methanol,” *Physical Chemistry Chemical Physics*, vol. 20, no. 16, pp. 11152–11159, 2018, doi: 10.1039/C8CP01476K.

[38] B. Wu *et al.*, “Fe binuclear sites convert methane to acetic acid with ultrahigh selectivity,” *Chem*, vol. 8, no. 6, pp. 1658–1672, Jun. 2022, doi: 10.1016/j.chempr.2022.02.001.

[39] J.-T. Han, H. Su, L. Tan, and C.-J. Li, “In aqua dual selective photocatalytic conversion of methane to formic acid and methanol with oxygen and water as oxidants without overoxidation,” *iScience*, vol. 26, no. 2, p. 105942, Feb. 2023, doi: 10.1016/j.isci.2023.105942.

[40] K. Zhu *et al.*, “Highly efficient conversion of methane to formic acid under mild conditions at ZSM-5-confined Fe-sites,” *Nano Energy*, vol. 82, p. 105718, Apr. 2021, doi: 10.1016/j.nanoen.2020.105718.

[41] Y. K. Krisnandi *et al.*, “The new challenge of partial oxidation of methane over Fe2O3/NaY and Fe3O4/NaY heterogeneous catalysts,” *Heliyon*, vol. 7, no. 11, p. e08305, Nov. 2021, doi: 10.1016/j.heliyon.2021.e08305.

[42] M. Tang, L. Xu, and M. Fan, “Progress in oxygen carrier development of methane-based chemical-looping reforming: A review,” *Appl Energy*, vol. 151, pp. 143–156, Aug. 2015, doi: 10.1016/j.apenergy.2015.04.017.

[43] Z. Zhou *et al.*, “Catalytic Partial Oxidation of Methane to Methanol over Fe2O3/MWCNTs,” *Catalysts*, vol. 14, no. 2, p. 134, Feb. 2024, doi: 10.3390/catal14020134.

[44] T. Al-Attas, K. Kannimuthu, M. A. Khan, and M. G. Kibria, “Uncovering Electrochemical Methane Oxidation Mechanism through the In Situ Detection of Reaction Intermediates,” *ACS Catal*, vol. 14, no. 14, pp. 10614–10623, Jul. 2024, doi: 10.1021/acscatal.4c00675.

[45] H. Zhang *et al.*, “Phase engineering of Fe2O3 nanocrystals for the direct oxidation of CH4 to HCOOH,” *J Catal*, vol. 432, p. 115452, Apr. 2024, doi: 10.1016/j.jcat.2024.115452.

[46] W. Zhou *et al.*, “Highly Selectively Methane Photooxidation to CH_3OH and HCHO over an Integrated Fe_2O_3/WO_3 Heterojunction Greatly Promoted by Iron(III) Chloride,” *ACS Catal*, vol. 14, no. 5, pp. 3606–3615, Mar. 2024, doi: 10.1021/acscatal.3c05391.

[47] M. B. Park, E. D. Park, and W.-S. Ahn, “Recent Progress in Direct Conversion of Methane to Methanol Over Copper-Exchanged Zeolites,” *Front Chem*, vol. 7, Jul. 2019, doi: 10.3389/fchem.2019.00514.

[48] K. Shen, S. Kumari, Y.-C. Huang, J. Jang, P. Sautet, and C. G. Morales-Guio, “Electrochemical Oxidation of Methane to Methanol on Electrodeposited Transition Metal Oxides,” *J Am Chem Soc*, vol. 145, no. 12, pp. 6927–6943, Mar. 2023, doi: 10.1021/jacs.3c00441.

[49] V. Vargheese, Y. Kobayashi, and S. T. Oyama, “The Direct Partial Oxidation of Methane to Dimethyl Ether over Pt/Y_2O_3 Catalysts Using an NO/O_2 Shuttle,” *Angewandte Chemie*, vol. 132, no. 38, pp. 16787–16793, Sep. 2020, doi: 10.1002/ange.202006020.

[50] X. Cui *et al.*, “Room-Temperature Methane Conversion by Graphene-Confined Single Iron Atoms,” *Chem*, vol. 4, no. 8, pp. 1902–1910, 2018, doi: 10.1016/j.chempr.2018.05.006.

[51] J. Nandenha, R. M. Piasentin, L. M. G. Silva, E. H. Fontes, A. O. Neto, and R. F. B. de Souza, “Partial oxidation of methane and generation of electricity using a PEMFC,” *Ionics (Kiel)*, vol. 25, no. 10, pp. 5077–5082, Oct. 2019, doi: 10.1007/s11581-019-03186-z.

[52] J. C. Fornaciari *et al.*, “A Perspective on the Electrochemical Oxidation of Methane to Methanol in Membrane Electrode Assemblies,” *ACS Energy Lett*, vol. 5, no. 9, pp. 2954–2963, Sep. 2020, doi: 10.1021/acsenergylett.0c01508.

[53] L.-C. Weng, A. T. Bell, and A. Z. Weber, “Towards membrane-electrode assembly systems for CO_2 reduction: a modeling study,” *Energy Environ Sci*, vol. 12, no. 6, pp. 1950–1968, 2019, doi: 10.1039/C9EE00909D.

[54] J. C. Fornaciari *et al.*, “A Perspective on the Electrochemical Oxidation of Methane to Methanol in Membrane Electrode Assemblies,” *ACS Energy Lett*, vol. 5, no. 9, pp. 2954–2963, Sep. 2020, doi: 10.1021/acsenergylett.0c01508.

[55] D. Higgins, C. Hahn, C. Xiang, T. F. Jaramillo, and A. Z. Weber, “Gas-Diffusion Electrodes for Carbon Dioxide Reduction: A New Paradigm,” *ACS Energy Lett*, vol. 4, no. 1, pp. 317–324, Jan. 2019, doi: 10.1021/acsenergylett.8b02035.

[56] K. Tabata *et al.*, “Activation of methane by oxygen and nitrogen oxides,” *Catalysis Reviews*, vol. 44, no. 1, pp. 1–58, Aug. 2002, doi: 10.1081/CR-120001458.

[57] S. J. Freakley, N. Dimitratos, D. J. Willock, S. H. Taylor, C. J. Kiely, and G. J. Hutchings, “Methane Oxidation to Methanol in Water,” *Acc Chem Res*, vol. 54, no. 11, pp. 2614–2623, Jun. 2021, doi: 10.1021/acs.accounts.1c00129.

[58] L. Luo *et al.*, “Water enables mild oxidation of methane to methanol on gold single-atom catalysts,” *Nat Commun*, vol. 12, no. 1, p. 1218, Feb. 2021, doi: 10.1038/s41467-021-21482-z.

[59] Z. Zuo, P. J. Ramírez, S. D. Senanayake, P. Liu, and J. A. Rodriguez, “Low-Temperature Conversion of Methane to Methanol on CeO_x/Cu_2O Catalysts: Water Controlled Activation of the C–H Bond,” *J Am Chem Soc*, vol. 138, no. 42, pp. 13810–13813, Oct. 2016, doi: 10.1021/jacs.6b08668.

[60] B. Lee, Y. Sakamoto, D. Hirabayashi, K. Suzuki, and T. Hibino, “Direct oxidation of methane to methanol over proton conductor/metal mixed catalysts,” *J Catal*, vol. 271, no. 2, pp. 195–200, May 2010, doi: 10.1016/j.jcat.2010.01.011.

[61] B. Lee and T. Hibino, “Efficient and selective formation of methanol from methane in a fuel cell-type reactor,” *J Catal*, vol. 279, no. 2, pp. 233–240, Apr. 2011, doi: 10.1016/j.jcat.2010.12.020.

[62] J. Nandenha, R. M. Piasentin, L. M. G. Silva, E. H. Fontes, A. O. Neto, and R. F. B. de Souza, “Partial oxidation of methane and generation of electricity using a PEMFC,” *Ionics (Kiel)*, vol. 25, no. 10, pp. 5077–5082, Oct. 2019, doi: 10.1007/s11581-019-03186-z.

[63] N. Spinner and W. E. Mustain, “Electrochemical Methane Activation and Conversion to Oxygenates at Room Temperature,” *J Electrochem Soc*, vol. 160, no. 11, pp. F1275–F1281, Oct. 2013, doi: 10.1149/2.071311jes.

[64] M. Ma, C. Oh, J. Kim, J. H. Moon, and J. H. Park, “Electrochemical CH4 oxidation into acids and ketones on ZrO2:NiCo2O4 quasi-solid solution nanowire catalyst,” *Appl Catal B*, vol. 259, p. 118095, Dec. 2019, doi: 10.1016/j.apcatb.2019.118095.

[65] J. Lee, J. Yang, and J. H. Moon, “Solar Cell-Powered Electrochemical Methane-to-Methanol Conversion with CuO/CeO_2 Catalysts,” *ACS Energy Lett*, vol. 6, no. 3, pp. 893–899, Mar. 2021, doi: 10.1021/acsenergylett.0c02553.

[66] C. Kim, H. Min, J. Kim, J. Sul, J. Yang, and J. H. Moon, “NiO/ZnO heterojunction nanorod catalyst for high-efficiency electrochemical conversion of methane,” *Appl Catal B*, vol. 323, p. 122129, Apr. 2023, doi: 10.1016/j.apcatb.2022.122129.

[67] J. Lee, S. Lee, C. Kim, J. S. Yoo, and J. H. Moon, “High-efficiency electrochemical methane conversion using Fe2O3-based catalysts assisted by thermochemical active oxygen,” *Appl Catal B*, vol. 344, p. 123633, May 2024, doi: 10.1016/j.apcatb.2023.123633.

[68] B. Scharifker, S. Eduvigis, O. Yepez, L. Carlota, J. Carlos De Jesus, and M. M. Ramirez De, “ELECTROCATALYTIC PROCESS.”

[69] M. C. L. Santos *et al.*, “Direct Alkaline Anion Exchange Membrane Fuel Cell to Converting Methane into Methanol,” *ChemistrySelect*, vol. 4, no. 39, pp. 11430–11434, Oct. 2019, doi: 10.1002/slct.201902421.

[70] B. Chen *et al.*, “Water–solid contact electrification causes hydrogen peroxide production from hydroxyl radical recombination in sprayed microdroplets,” *Proceedings of the National Academy of Sciences*, vol. 119, no. 32, Aug. 2022, doi: 10.1073/pnas.2209056119.

[71] X. Song, C. Basheer, and R. N. Zare, “Water Microdroplets-Initiated Methane Oxidation,” *J Am Chem Soc*, vol. 145, no. 50, pp. 27198–27204, Dec. 2023, doi: 10.1021/jacs.3c08643.

[72] J. Li, J. Xu, Q. Song, X. Zhang, Y. Xia, and R. N. Zare, “Methane C(sp ^{3})–H bond activation by water microbubbles,” *Chem Sci*, vol. 15, no. 41, pp. 17026–17031, 2024, doi: 10.1039/D4SC05773B.

[73] J. Deng *et al.*, “Chemical looping conversion of methane via Fe2O3-LaFeO3 calcined from LaFe-MOF precursor,” *Chin J Chem Eng*, vol. 62, pp. 225–237, Oct. 2023, doi: 10.1016/j.cjche.2023.04.002.

[74] C. M. Godoi *et al.*, “Methane conversion to higher value-added product and energy co-generation using anodes OF PdCu/C in a solid electrolyte reactor: alkaline fuel cell type monitored by differential mass spectroscopy,” *Research on Chemical Intermediates*, vol. 47, no. 2, pp. 743–757, Feb. 2021, doi: 10.1007/s11164-020-04296-4.

[75] Z. Zhou *et al.*, “Catalytic Partial Oxidation of Methane to Methanol over Fe2O3/MWCNTs,” *Catalysts*, vol. 14, no. 2, p. 134, Feb. 2024, doi: 10.3390/catal14020134.

[76] J. Deng *et al.*, “Chemical looping conversion of methane via Fe2O3-LaFeO3 calcined from LaFe-MOF precursor,” *Chin J Chem Eng*, vol. 62, pp. 225–237, Oct. 2023, doi: 10.1016/j.cjche.2023.04.002.

[77] X. Song, C. Basheer, J. Xu, M. M. Adam, and R. N. Zare, “Methane Bubbled Through Seawater Can be Converted to Methanol With High Efficiency,” *Advanced Science*, 2024.

[78] A. H. Bagherzadeh Mostaghimi, T. A. Al-Attas, M. G. Kibria, and S. Siahrostami, “A review on electrocatalytic oxidation of methane to oxygenates,” *J Mater Chem A Mater*, vol. 8, no. 31, pp. 15575–15590, 2020, doi: 10.1039/D0TA03758C.

VITAE

Name: Muhammad Mustapha Adam.

Nationality: Nigerian.

Date of Birth :10/26/1998.

Email: mmadam1042@gmail.com

Address: No. 2, Opposite GDCSS, Tudunwada K, Gombe, Nigeria.

Academic Background: BSc chemistry, Gombe State University, 2019